Contrib Mineral Petrol (2007) 153:1–28
DOI 10.1007/s00410-006-0130-3

ORIGINAL PAPER

Garnet reequilibration and growth in the eclogite facies and geodynamical evolution near peak metamorphic conditions

Hugues Raimbourg · Bruno Goffé · Laurent Jolivet

Received: 11 May 2005 / Accepted: 26 July 2006 / Published online: 5 September 2006

Abstract Caledonian eclogite-facies metamorphism partially reworking Grenvillian granulite-facies anorthosite allows us to study the processes of garnet reequilibration at high pressure and to reconstruct the evolution of the unit near metamorphic peak conditions. Our results indicate that eclogite-facies metamorphism happened in two successive phases: first, inherited granulitic garnet was fractured and reequilibrated from their boundaries (crystal or fracture rims); then eclogite-facies minerals were crystallised in the fractures as overgrowths on inherited garnets. The reequilibration of inherited garnets is achieved through $Fe^{2+}Mg^{-1}$ exchange, whereas eclogite-facies garnets crystallised during the subsequent phase are notably richer in Ca than un- and re-equilibrated granulitic garnet. Pseudosection construction shows that this lack in Ca reequilibration cannot be related to variations in thermodynamic conditions (a_{H2O}, reacting system composition) between the two phases. From the compilation of the available data, the reequilibration of granulitic garnet seems to be controlled by the inefficient intra- and inter-granular transport properties of Ca compared to Fe^{2+} and Mg. While these kinetic factors confine garnet reequilibration to $Fe^{2+}Mg^{-1}$ exchange, the extent of reequilibration along this exchange vector is controlled by partitioning with adjacent omphacite. On the contrary to the diffusional reequilibration of granulitic garnet that lasted for several My according to our modelling of the diffusional relaxation, the strong compositional gradients between eclogite-facies and reequilibrated garnets, which are almost unaffected by diffusional reequilibration, provide evidence that rapid exhumation followed the crystallisation of eclogite-facies minerals. We propose that the movement reversal itself, from burial to exhumation, and associated deformation and fluid flow, triggered this crystallisation event. The resulting evolution near metamorphic peak conditions is therefore strongly asymmetrical: on the one hand, the prograde diffusional relaxation profiles indicate slow movement during the last stages of burial, whereas the unaffected retrograde overgrowth indicates fast exhumation rates.

Communicated by J. Hoefs.

H. Raimbourg (✉)
Department of Earth and Planetary Science,
Graduate School of Science, The University of Tokyo,
Science Build. 1, 7-3-1 Hongo, Bunkyo-ku,
Tokyo 113-0033, Japan
e-mail: hraimbou@eps.s.u-tokyo.ac.jp

B. Goffé
Laboratoire de Géologie, Ecole Normale Supérieure,
Paris, France

L. Jolivet
Laboratoire de Tectonique,
Université Pierre et Marie Curie, Paris, France

Introduction

Garnet is ubiquitous in high pressure metamorphic rocks, and is used to determine *P*–*T* conditions—for example with garnet-hornblende (Krogh Ravna 2000a), garnet-clinopyroxene (Ai 1994; Berman et al. 1995; Powell 1985) geothermometers or with the garnet–clinopyroxene–phengite geobarometer (Waters and Martin 1993)—as well as rates of tectonometamorphic processes (Cristensen et al. 1989; Dachs and

Proyer 2002; Hauzenberger 2005; Lasaga 1983; Vance and O'Nions 1990) or growth controlling parameters (Carlson 1989; Konrad-Schmolke et al. 2005; O'Brien 1999).

The hypothesis underlying all such studies is the low cation diffusivities within garnet with respect to geological evolution, which results in the preservation of compositionally inhomogeneous garnets. Although often unable to reset garnet compositions completely, the effect of retrograde partial diffusive reequilibration must nevertheless be accounted for in order to assess correct peak compositions. But partial reequilibration in itself contains information about evolution after the crystallisation: modelling of diffusion profiles yields duration estimates of metamorphic overprint (O'Brien and Vrana 1995) or exhumation (Perchuk et al. 1999). Besides, diffusive reequilibration of garnet in radiogenic elements, which controls the closure temperature (Dodson 1973; Ganguly and Tirone 1999), is crucial to interpret radiogenic ages (Burton and O'Nions 1991; Getty et al. 1993; Mezger et al. 1989; Vance et al. 1998).

Cations diffusivities within garnets have been assessed for a various range of *P*–*T* conditions and garnet compositions, on the basis of experiments (Bejina et al. 2003; Chakraborty and Ganguly 1992; Chakraborty and Rubie 1996; Cygan and Lasaga 1985; Elphick et al. 1985; Freer and Edwards 1999; Ganguly et al. 1998; Loomis et al. 1985; Schwandt et al. 1995, 1996) or of natural samples data (Dachs and Proyer 2002; Ganguly et al. 1996). Results of this modelling are sometimes slightly disagreeing (see Freer and Edwards 1999; Schwandt et al. 1996 for Ca diffusivity) due to the complexity of theoretical modelling of ternary or quaternary diffusional system (for example Chakraborty and Ganguly 1992), and to the large possible compositional range of analysed garnets.

Actual reequilibration in natural garnets results not only from intra-garnet diffusion but also from the combination of garnet interface processes and intergranular fluid-mediated cations transport (Dohmen and Chakraborty 2003). Furthermore, element fractionation, resulting in strong compositional gradients during garnet growth (Chernoff and Carlson 1997; Elvevold and Gilotti 2000; Hollister 1966; Indares 1995; Konrad-Schmolke et al. 2005; Loomis 1982; Marmo et al. 2002; O'Brien 1997), can also affect reequilibration patterns as in the case where temperature changes modify the garnet diffusing volume (Stüwe 1997). All these elementary mechanisms must be analysed in order to get a better insight into garnet reequilibration, and from there on into geodynamical evolution at depth.

The samples studied here belong to the Lindås nappe, in the Bergen Arcs, Norway. The rock is a granulite facies anorthosite that was deformed and partially reequilibrated under eclogite-facies conditions during the Caledonian orogenesis (Austrheim 1987; Austrheim and Griffin 1985). Deformation caused brittle fracturing of the inherited (granulitic) garnet grains, which enabled diffusional reequilibration of the garnet composition along fracture sides. During a later stage, open fractures were filled by eclogite-facies minerals such as omphacite, phengite and garnet.

We present evidence that eclogite-facies reequilibration of inherited granulitic garnets resulted mainly from Fe^{2+}–Mg^{-1} exchange, barely affecting the very low grossular content, whereas garnets newly grown in the eclogite-facies field contain significant amount of grossular component. The use of pseudosection analysis shows that neither variations in water activity nor in reacting bulk composition can explain the observed compositional variations in garnet along a reasonable *P*–*T* path. We propose that lacking diffusional reequilibration of Ca along fracture sides is kinetically controlled by intra- and inter-granular transport properties of cations.

Our analysis of high-pressure garnet generations led us to decompose the eclogite-facies event in two successive phases limited by eclogitic garnet crystallisation. The diffusion profiles associated with the two phases (first inherited garnet reequilibration, then eclogitic garnet-inherited garnet inter-diffusion) show very inequal durations and evidence that eclogite-facies garnet crystallisation was rapidly followed by exhumation. We propose to relate these successive garnet generations to the reversal of the crustal sliver motion from burial to exhumation.

Geological and petrological settings

The meta-anorthosite unit studied on the northwest of Holsnøy island is part of the Lindås nappe, which belongs to the Bergen Arcs, a pile of arcuate nappes centered around Bergen, Norway (Kolderup and Kolderup 1940) (Fig. 1). The meta-anorthosite has experienced two main metamorphic events: it was completely recrystallised under granulite facies conditions during the Grenvillian orogenesis around 900 Ma (Bingen et al. 2001; Cohen et al. 1988), <10 kbars and 800–850°C (Austrheim 1987) and experienced eclogite facies metamorphism during the Caledonian orogenesis around 460–420 Ma (Bingen et al. 2004; Boundy

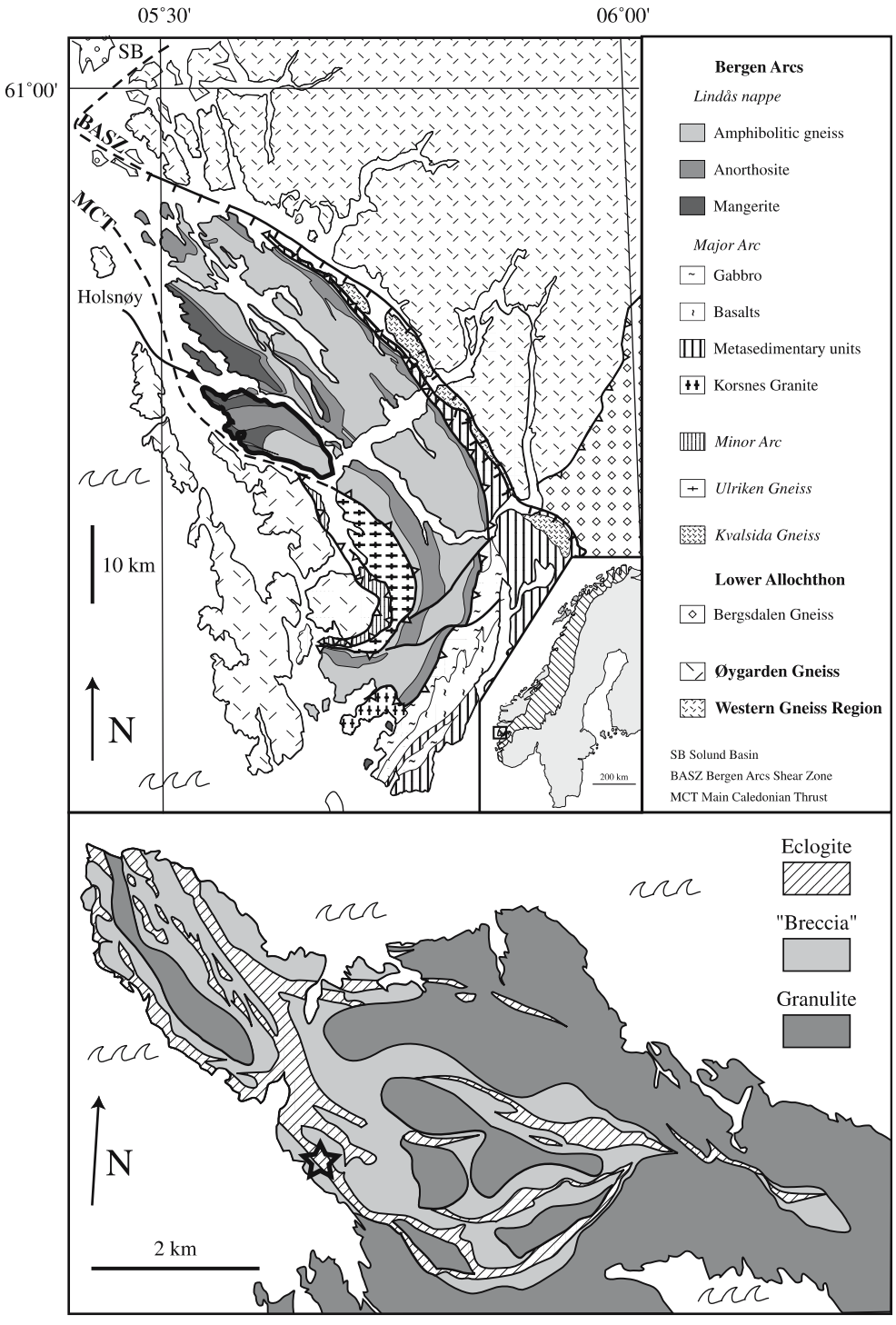

Fig. 1 *Top* Geological map of the Bergen Arcs (Ragnhildsveit and Helliksen 1997). General map of Norwegian Caledonides by Roberts and Gee (1985). *Bottom* Northwestern Holsnøy from Austrheim et al. (1997) and Boundy et al. (1997a), with heterogeneous distribution of eclogitic overprint on granulite. Eclogite, Breccia and Granulite correspond respectively to degrees of eclogitic metamorphism >80, 40–80, <40%. Rock sampling is located by the *star*

et al. 1996, 1997b; Cohen et al. 1988; Glodny et al. 2002), >19 kbars and 700–750°C (Jamtveit et al. 1990; this study). It was subsequently affected by amphibolite-facies (Boundy et al. 1996; Kühn 2002) and greenschist-facies (Schmid et al. 1998) metamorphism during its exhumation path.

Fluid influx into the anorthositic unit is necessary to trigger the transformation of the almost anhydrous granulite into eclogite (Austrheim 1987, 1990, 1998). Limited influx of fluid resulted in the juxtaposition of metastably preserved and variably eclogitised granulite (Austrheim 1990; Boundy et al. 1992). Macroscopically, in the least transformed areas, eclogitisation occurs in dm-wide bands on both sides of scattered *m*-long fractures filled with hydrous eclogitic minerals, cutting through pristine granulite (Fig. 2). In the most

transformed areas, the granulite is only preserved in metre-sized boudins within decameter-wide eclogitic shear zones.

The typical granulite-facies assemblage is plagioclase, diopside, garnet, +/ – scapolite, +/ – orthopyroxene, +/ – hornblende (Austrheim and Griffin 1985; Kühn 2002). The granulite has a local coronitic texture, made of elongated aggregates of garnet and pyroxenes embedded in a plagioclase matrix. In the least reacted samples, eclogitisation consists only of ~15 μm sized aggregates of K-feldspar, kyanite and zoisite formed along grain boundaries. In slightly more hydrated samples, plagioclase grains show fine intergrowths of kyanite, zoisite and phengite needles (Kühn 2002). The equilibrium eclogite-facies assemblage is visible on the most eclogitised samples, with omphacite, eclogitic garnet, phengite, zoisite, kyanite, quartz, +/ – amphibole, +/ – paragonite, +/ – calcite, +/ – dolomite (Austrheim and Griffin 1985; Kühn 2002) (Fig. 3).

Eclogitisation is heterogeneous even at sample scale (Fig. 2) and centimetre-sized areas of typical eclogite facies minerals coexist with areas of pristine granulitic minerals. Garnet is particularly resistant to reequilibration, and even in the most transformed and deformed samples, which were collected in eclogitic shear zones, many garnets are inherited from the granulitic assemblage and reequilibrate only on the rim and along fractures.

Eclogite facies garnet variety

In the following observations, ''granulitic garnet'' refers to garnets inherited from ante-caledonian metamorphism, either unequilibrated (grt I) or partially reequilibrated (grt II) during the Caledonian high-pressure event, while ''eclogitic garnet'' or ''grt III'' refers to garnets grown during this high-pressure phase (Fig. 4). While partially reequilibrated granulitic garnets are typically 1 mm large and euhedral, the garnets grown in the eclogite-field are either rare ~100 μm large euhedral garnets or more abundant overgrowths on the granulitic garnet. These eclogitic garnets do not show any compositional zoning.

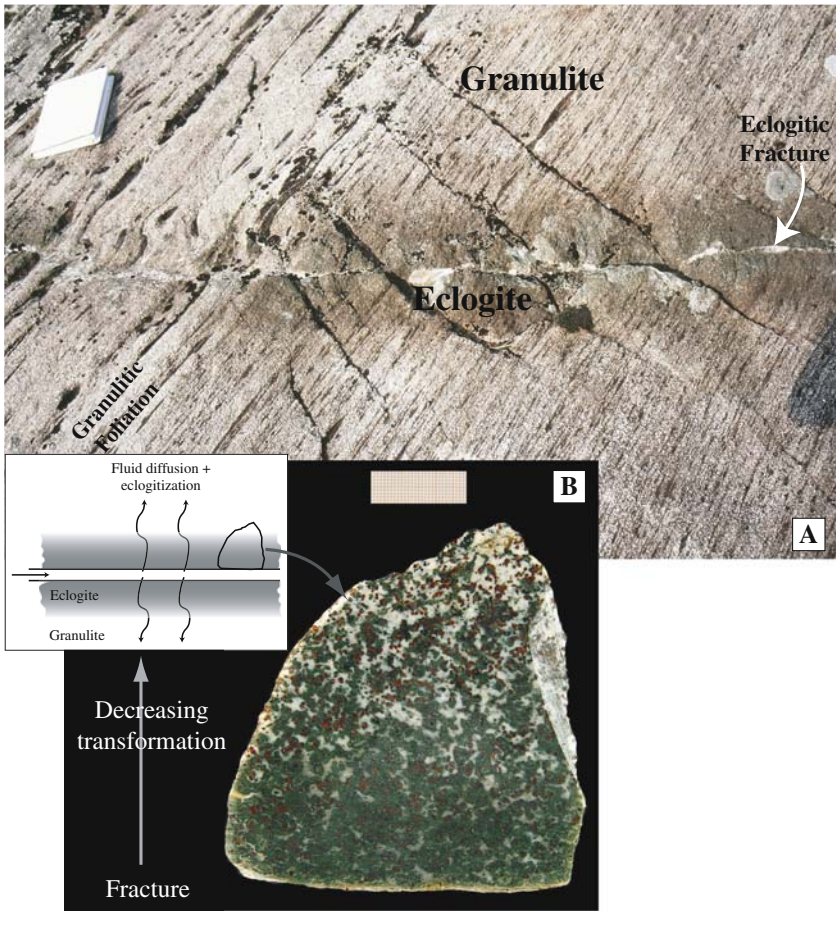

Fig. 2 **a** Eclogite facies reaction zone along metres-long fractures filled with hydrous minerals that cut through granulite. Macroscopic deformation is visible in the eclogitic zone as the granulitic foliation is slightly deflected. **b** Photograph of a section of rock sampled next to a macroscopic fracture. The fluid diffused from the macroscopic fracture into the host granulite. Its concentration gradient resulted in the decrease in the extent of eclogitisation from the fracture, visible at the sample scale

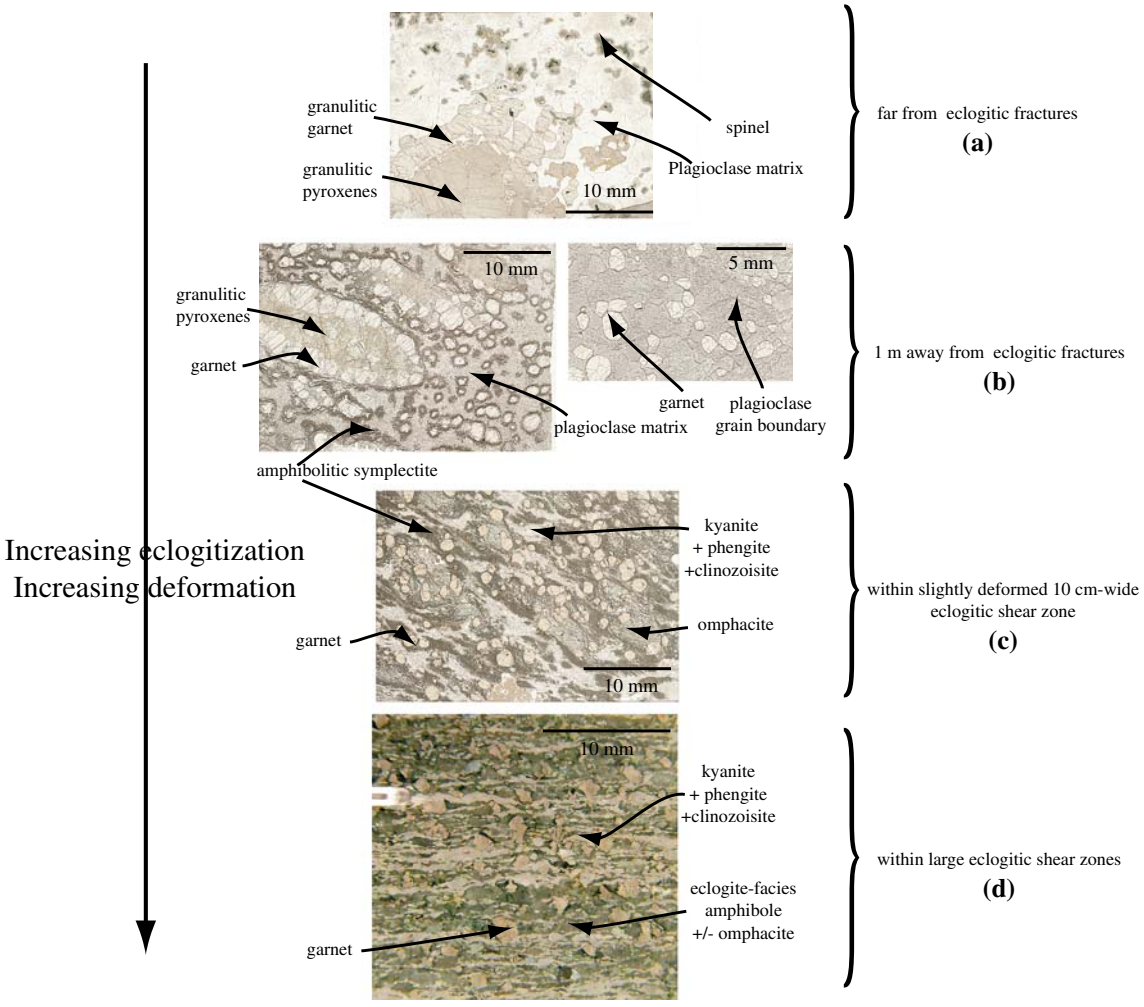

Fig. 3 Photographs of thin sections, showing increasing eclogitisation. Samples (**a**), (**b**) and (**c**) are located in ''granulite'' zones of Fig. 1, where eclogitisation is present as deformed and undeformed reaction zones along metres-long fractures in pristine granulite. In the macroscopically uneclogitised granulite, eclogitisation started along grain boundaries as thin needles of phengite, kyanite and clinozoisite growing within plagioclase. Within the 10 cm-wide macroscopic eclogitic reaction zone, the only remaining granulite facies minerals are garnets, but the granulitic coronitic texture is still preserved as omphacite–garnet aggregates (former mafic coronas) embedded in kyanite–phengite–clinozoisite matrix (former plagioclase matrix). This eclogitised reaction zone started to deform, causing the elongation of the aggregates, first step in the acquisition of an eclogitic foliation. In sample (**d**), stemming from a large eclogitic shear zone, the eclogitic foliation is fully developed with alternating layers of kyanite–phengite–clinozoisite and omphacite–amphibole–garnet, crosscut by a dextral shear zone roughly from top left to bottom right. Note that due to a different bulk composition, eclogitic paragenesis comprises very little amphibole and much omphacite in sample (**c**), on the contrary to the dark layers of sample (**d**) that are mainly made of amphibole and minor omphacite. Note the overprint of amphibolitisation as dark amphibolitic symplectites of plagioclase + amphibole on samples (**b**) left and (**c**)

Trails of eclogitic inclusions and reequilibrated garnet

In highly transformed samples, most inherited granulitic garnets are crosscut by 10–100 μm wide bands showing enrichment in almandine component (grt II) (Fig. 5). Some of these bands are located on both sides of mineral-filled veins (omphacite, amphibole, phengite, kyanite, quartz, dolomite), or trails of inclusions (Erambert and Austrheim 1993). According to these authors, garnet fracturing was followed by fluid and element transport within fractures, fracture sides reequilibration and eventually crystallisation of aligned eclogitic inclusions.

In addition to the reequilibration along fractures, rims of inherited granulitic garnets from eclogitised

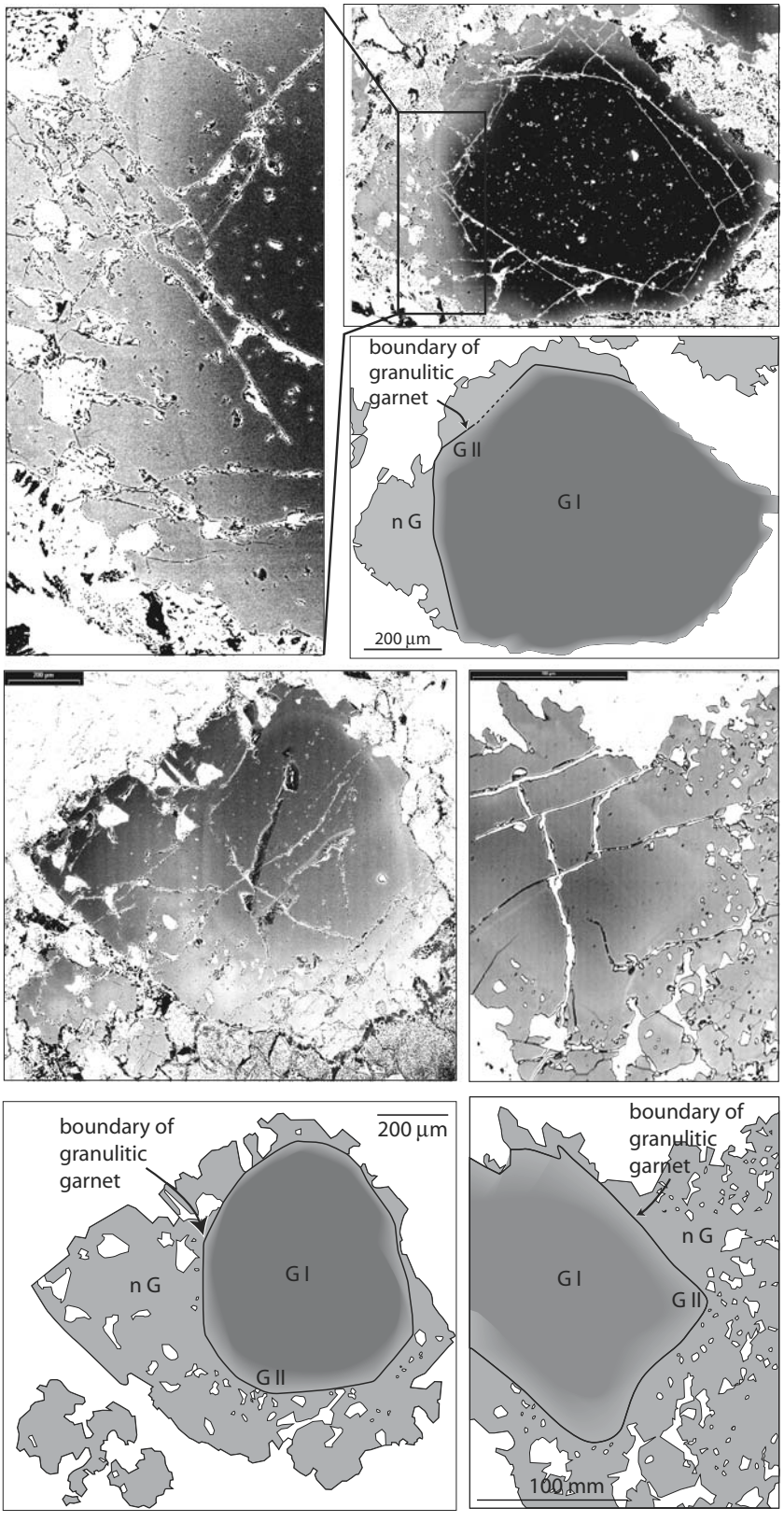

Fig. 4 BSE photographs of inherited granulitic garnets that are heterogeneously reequilibrated and locally surrounded by eclogitic garnet overgrowths. The limit between the two garnets is a relatively straight line corresponding to the rim of the euhedral inherited granulitic garnet. On the inner side of this border, the granulitic garnet is reequilibrated within a bright band up to 50 µm wide. The brightness of this reequilibrated garnet decreases progressively to reach core values, corresponding to the fact that the chemical composition, hence the reequilibration extent, is continuous from rim to core. The grey levels distribution curve is narrow and centered around garnet, in order to see garnet mass heterogeneities, as a result most of the other minerals appear white. While the granulitic garnet, either reequilibrated or not, is inclusion-free, the eclogitic garnet overgrowths contain many inclusions. Note that due to a problem in device adjustment, a brightness gradient is superposed to mass contrast signal on image 3, with brightness increasing from top left to bottom right

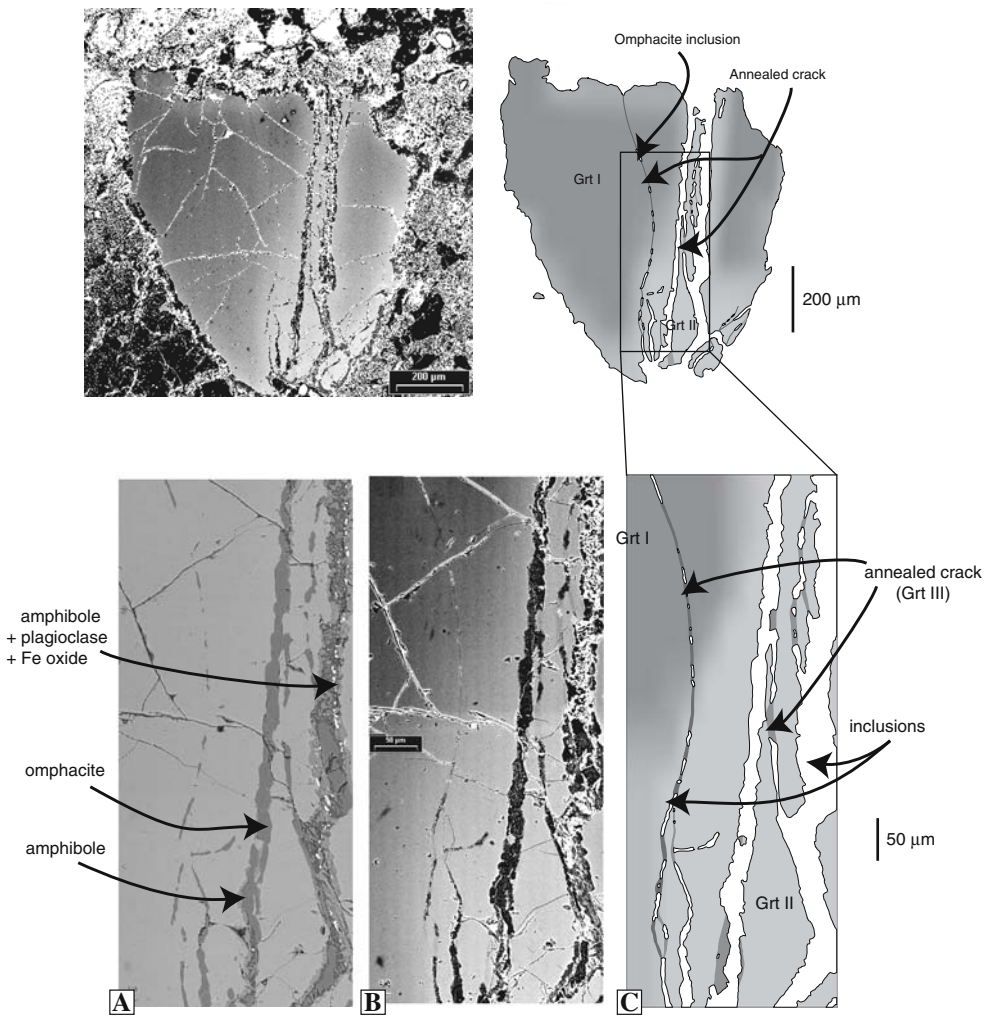

Fig. 5 BSE photographs of eclogitic fractures filled with eclogite facies-minerals and surrounded by a bright band of reequilibrated granulitic garnet (grt II). In **a** the grey level spectrum is wide, in order to see the different inclusions, while in **b** the spectrum is narrower to see garnet mass contrast. The granulitic garnet has preserved granulitic composition far from the vein and is increasingly reequilibrated towards the vein. In addition, apparently isolated omphacite inclusions are linked with one another by micrometre-wide darker garnet (grt III f) annealing the former cracks. The large vein on the right of the bottom photographs has been partially retrogressed in the amphibolite facies into a plagioclase + amphibole + Fe-oxide assemblage

samples are similarly enriched in almandine on a variable width (up to 100–150 µm) (Fig. 4). Almandine-rich stripes along fractures are similar to almandine-enriched garnet rims: fractures act as new grain boundaries where granulitic garnets react.

If fractures-filling minerals are typical eclogite-facies assemblages, it is difficult to assess the conditions of fracturing itself, prior to mineral crystallisation. Nevertheless, garnet fracturing and subsequent reequilibration are likely to be associated also with the eclogite-facies event, as fractures with reequilibrated sides as well as reequilibrated garnet rims are absent from uneclogitised zones, while fracture density and reequilibration widths are highest in eclogite-facies shear zones, where the transformation to eclogite is the most complete and deformation is the most intense (Erambert and Austrheim 1993).

Reequilibrated granulitic versus grown eclogitic garnet

Whether a garnet was reequilibrated from a previous generation (involving only cation diffusion in an existing crystallographic structure) or was newly grown was determined from the comparison of almost untransformed samples with eclogitised ones. The garnets in eclogitised samples (Fig. 4) have a core of granulitic composition (grt I: $Alm_{47}Gr_{15}Py_{38}$) which gets smoothly almandine richer towards the rim (grt II: $Alm_{57}Gr_{18}Py_{25}$). The grt II and the outermost garnet

(grt III: $Alm_{50}Gr_{26}Py_{24}$), compositionally much different, are separated by a sharp and straight boundary (profiles are shown later in Fig. 10). This straight boundary reproduces the shape of euhedral granulitic garnet in uneclogitised samples. In addition, grt II is always inclusion-free, while eclogite-facies inclusions are localised either at the grt II–III boundary or within grt III. It is therefore likely that grt II is a reequilibrated garnet, while grt III is an overgrowth that was formed in the eclogite-facies *P–T* field.

The comparison of the compositions of the preserved granulitic (grt I) and reequilibrated garnet (grt II) shows that the reequilibration in the eclogite-facies *P–T* conditions proceeds mainly through a Fe^{2+}–Mg exchange, the grossular fraction being roughly constant. In contrast, garnets grown during the eclogite-facies event (grt III) are significantly enriched in grossular component.

Annealed eclogitic fractures in granulitic garnet

The alignment of eclogitic inclusions, as well as the parallel band of grt II was used as an evidence for eclogite facies fracturing but later annealing was also assumed, as no present fracture is actually linking the inclusions (Erambert and Austrheim 1993). The BSE study of some granulitic garnets shows a thin band (1–10 μm) of garnet slightly darker than the surrounding grt II, connecting the eclogitic inclusions, in the middle of the large band of light grt II (Fig. 5). This garnet (grt III f) has a composition very close to the overgrowths of eclogitic garnets (grt III r) on the rim of granulitic garnets, and is sometimes connected to it (Fig. 6). It is interpreted as filling in the space between both sides of the fractures, in the same respect as other inclusions, but is indistinguishable from host garnet with optical microscopy and is visible with the BSE only when focusing on garnet mass contrast. All the samples showing fractures annealed with grt III f were collected in a small geographical area (500 × 500 m) in the breccia zone, while the three samples collected elsewhere, within large shear zones, do not have grt III f.

Two sets of eclogite facies garnet compositions

The observations above lead to the subdivision of garnets in two sets, corresponding either to reequilibrated garnet (grt II), or to garnet grown in the eclogite-facies (overgrowth on the rim of granulitic garnet—grt III r—or fracture infill—grt III f). This sorting corresponds to compositional differences in pyrope, grossular and almandine fractions. These two kinds of garnets are nevertheless associated with the eclogite facies *P–T* conditions, as they are not present in uneclogitised granulitic samples, and closely associated to eclogite-facies fractures.

Eclogite facies petrography

Mineral chemistry

All the following minerals were analysed with the electronic microprobe described in Appendix. In addition to eclogite-facies' minerals compositions, characteristic granulite-facies minerals are also described in Table 1 (see also Austrheim and Griffin 1985; Kühn 2002).

Garnets grown at eclogite-facies conditions are systematically enriched in Ca with respect to inherited granulite facies garnets. Nevertheless, depending on the nature of the protolith, whose composition ranges from anorthosite to gabbro (Austrheim and Griffin 1985), eclogitic garnet (grt III) is not always present. In the samples with grt III, the characteristic eclogite-facies paragenesis is composed of omphacite, garnet, phengite, clinozoisite. High-pressure amphibole (Table 1), although present in minor amounts in some eclogite samples (Austrheim and Mørk 1988; Boundy et al. 1992), was never observed coexisting with grt III, and is therefore not considered in the following thermobarometric analyses (for further description of eclogites-facies reaction involving amphiboles see Austrheim 1987; Kühn 2002).

In the samples where grt III f is present in fracture cores, coexisting inclusions are mainly omphacite and phengite. Additional minute inclusions of quartz and dolomite are present. The size of omphacite and phengite is variable, from 1 to 50 μm, and most inclusions are elongated in the direction of the fracture.

Omphacite

Omphacite was decomposed using the six end-members acmite, jadeite, diopside, hedenbergite, Fe/Mg pyroxene and Ca-Tschermak pyroxene. The projection onto the triangle jadeite–hedenbergite–diopside (Fig. 7) shows that the proportion of hedenbergite is relatively constant around 10%. The jadeitic substitution $NaAlCa^{-1}(FeMg)^{-1}$ is clustered in the range 50–70%. The isolated points outside this range may correspond to partially reequilibrated granulitic pyroxene. On the second triangular diagram the hedenbergite end-member is replaced by acmite, and the $Fe^{3+}Al^{-1}$ substitution is concentrated in the range 0–20%. In both diagrams

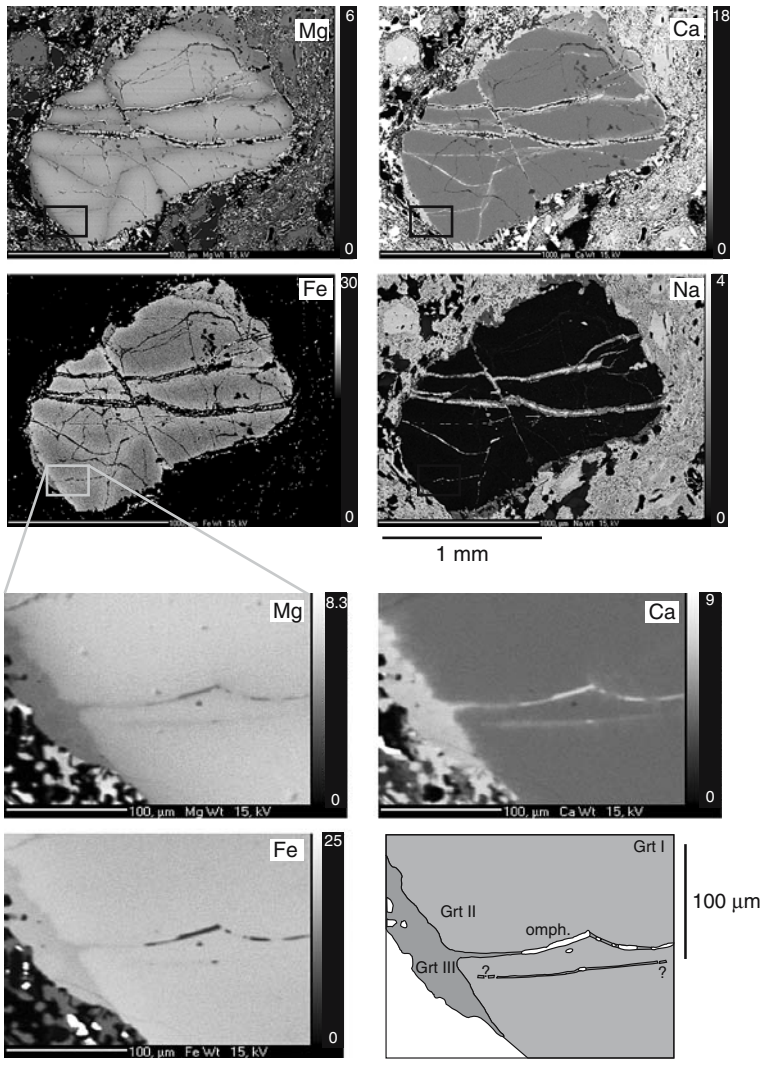

Fig. 6 Electron microprobe quantitative element map of a fractured granulitic garnet. The eclogitic fractures correspond either to large veins cutting through the garnet, or to discontinuous trails of omphacite inclusions (marked by high-Na content) linked by grt III f, both marked by bands of reequilibrated grt II on their sides. The reequilibration of the granulitic garnet consists in Mg-depletion and Fe-enrichment. The granulitic garnet is also surrounded on its SW and NE sides by eclogitic overgrowths, which are richer in Ca than grt I and II, and variably enriched in Fe compared to grt I, but less than grt II. The bottom zoom shows than grt III f within the crack has a composition close to the garnet overgrowth grt III r and is connected to it. The scale bar on the sides of each photograph is the percentage of oxide weight (MgO, FeO, CaO and Na_2O)

there is no significant difference between eclogitic pyroxene in the matrix and in inclusions within garnet.

Phengite

Phengite was decomposed using the five end-members trioctaedric mica, pyrophyllite, muscovite, celadonite and paragonite. The projection on the triangle ferroceladonite–magnesioceladonite–muscovite (Fig. 8) shows that the substitution $FeMg^{-1}$ is relatively constant around 50%. The phengitic substitution $X^2SiAl^{-1}Al^{-1}$, where X is either Fe or Mg, is concentrated in the range 15–25%, corresponding respectively to stoechiometric $Si_{3,15}$ and $Si_{3,25}$. The comparison of the three sets of analysed mica—the inclusions of mica within granulitic garnet, the micas on the rim of granulitic garnets and the micas in the matrix—do not show any systematic deviation.

Garnet

Triangular decomposition Garnet was decomposed using the four end-members: almandine, grossular, pyrope and spessartine. To determine the proportion of almandine, we assessed first the proportion of Fe^{3+} in the Fe_{total} analysed using the stoechiometric method developed by Droop (1987). The proportion of spessartine being always less than 3%, all the following garnet compositions are projected into the almandine–pyrope–grossular triangle (Fig. 9).

Granulitic garnet (grt I) The granulitic garnet has relatively homogeneous compositions around $Alm_{47}Gr_{15}Py_{38}$ (Fig. 9).

Reequilibrated granulitic garnet (grt II) The grt II is granulitic garnet reequilibrated by diffusion from rim (either granulitic garnet original boundary or fracture

Table 1 Representative electron-microprobe analyses of granulite- and eclogite-facies minerals. Normalisation of structural formulae is made over 8, 12, 6, 11, 23 and 25 atoms of oxygens for plagioclase, garnet, pyroxene, phengite, amphibole and clinozoisite, respectively

Gran. Facies

Mineral		pl	pl		px	px	px		Grt I	Grt I	Grt I
Sample		G01-II	G01-II		L02b-gt21	L02b-gt22	G01-s6		C01-gt7-V	E01-gt12-V	G01-pt7-II
Analyse		9 / 1 .	33 / 1 .		20_6	21_30	27,00		61 / 1 .	94 / 1 .	25 / 1 .
SiO2		62,23	58,38		51,42	51,97	48,84		39,48	39,27	41,52
TiO2		0,02	0,07		0,26	0,72	0,92		0,11	0,10	0,25
Al2O3		23,50	25,57		6,09	5,66	11,23		21,46	21,46	21,33
FeO		0,04	0,06		7,82	7,92	5,92		23,97	24,76	15,02
MnO		0,05	-0,01		0,14	0,04	0,03		0,75	0,80	0,24
MgO		0,00	0,00		11,65	11,44	10,52		9,80	9,53	13,71
CaO		4,81	8,69		21,24	20,26	20,27		5,37	5,79	7,74
Na2O		8,77	6,94		1,70	2,20	2,15		0,02	0,01	0,00
K2O		0,29	0,30		0,02	0,00	0,03		-0,01	-0,02	0,01
S		99,72	100,00		100,34	100,19	99,89		100,95	101,69	99,81
Structural Formulae											
Si		2,77	2,62		1,90	1,92	1,79		3,00	2,97	3,06
Ti		0,00	0,00		0,01	0,02	0,03		0,01	0,01	0,01
Al		1,23	1,35		0,27	0,25	0,49		1,92	1,92	1,85
Fetot		0,00	0,00		0,24	0,24	0,18		1,52	1,57	0,93
Mn		0,00	0,00		0,00	0,00	0,00		0,05	0,05	0,01
Mg		0,00	0,00		0,64	0,63	0,58		1,11	1,08	1,51
Ca		0,23	0,42		0,84	0,80	0,80		0,44	0,47	0,61
Na		0,76	0,60		0,12	0,16	0,15		0,00	0,00	0,00
K		0,02	0,02		0,00	0,00	0,00		0,00	0,00	0,00
Cr		0,00	0,00		0,00	0,00	0,00		0,00	0,00	0,00
XMg		0,02	-0,17		0,72	0,72	0,76		0,41	0,40	0,62
Endmembers	Xan	0,23	0,40	acm	0,07	0,07	0,07	Grs	0,15	0,16	0,20
	Xab	0,75	0,58	jd	0,05	0,09	0,09	Prp	0,37	0,36	0,49
	XK	0,02	0,02	hd	0,13	0,13	0,07	Alm	0,47	0,46	0,30
				di	0,60	0,59	0,53	Sps	0,02	0,02	0,00
				fe mg Px	0,04	0,04	0,05				
				Ca tsch	0,11	0,08	0,20				

Eclo. Facies

Mineral		Grt IIIf	Grt IIIf	Grt IIIr	Grt II	Grt II	Grt II		Ph next to gt	Ph next to gt	Ph inclus.	Ph inclus.	Ph matrix	Ph matrix
Sample		L02-Gt9-7	E01-gt12-V	E01-gt9-V	L02-Gt29-6	C01-Gt7-5	J01-Gt13-7		E01-gt3	E01-gt3	C01-s2	F01-gt17-7	C01-s3	E01-s1
Analyse		76/1.	97/1.	141 / 1 .	15/1.	59/1.	13/1.		75/14	76/28	18,00	22 / 1 .	46 / 1 .	34./1
SiO2		38,22	39,51	38,92	39,23	38,39	37,55		47,77	49,08	47,99	46,79	50,35	47,31
TiO2		0,07	0,05	0,26	0,10	0,04	0,05		0,56	0,33	1,02	0,38	0,99	0,32
Al2O3		21,18	21,75	21,70	21,21	20,92	20,55		32,86	29,71	32,07	30,23	30,35	32,86
FeO		24,23	23,85	24,84	24,47	26,92	28,03		2,68	3,44	3,00	2,82	2,63	2,59
MnO		1,02	0,86	0,83	0,90	1,05	1,21		0,08	0,22	0,07	0,06	0,05	0,00
MgO		5,16	6,88	6,67	8,73	6,80	6,19		1,55	2,50	1,83	2,40	1,65	1,60
CaO		10,04	8,95	8,46	5,59	7,21	5,97		0,10	1,10	0,08	0,07	0,00	0,06
Na2O		0,10	0,07	0,10	0,03	0,05	0,05		1,00	2,65	1,24	0,68	1,80	1,12
K2O		0,08	0,01	-0,01	-0,01	-0,03	-0,01		9,62	7,54	9,04	10,23	8,67	9,46
S		100,08	101,92	101,76	100,25	101,35	99,58		96,22	96,54	96,34	93,66	96,48	95,32
Structural Formulae														
Si		2,98	3,00	2,97	3,01	2,97	2,97		3,16	3,24	3,17	3,20	3,30	3,15
Ti		0,00	0,00	0,01	0,01	0,00	0,00		0,03	0,02	0,05	0,02	0,05	0,02
Al		1,95	1,95	1,95	1,92	1,91	1,92		2,56	2,31	2,50	2,44	2,34	2,58
Fetot		1,58	1,51	1,59	1,57	1,74	1,86		0,15	0,19	0,17	0,16	0,14	0,14
Mn		0,07	0,06	0,05	0,06	0,07	0,08		0,00	0,01	0,00	0,00	0,00	0,00
Mg		0,60	0,78	0,76	1,00	0,78	0,73		0,15	0,25	0,18	0,25	0,16	0,16
Ca		0,84	0,73	0,69	0,46	0,60	0,51		0,01	0,08	0,01	0,00	0,00	0,00
Na		0,01	0,01	0,01	0,00	0,01	0,01		0,13	0,34	0,16	0,09	0,23	0,14
K		0,01	0,00	0,00	0,00	0,00	0,00		0,81	0,64	0,76	0,89	0,73	0,80
Cr		0,00	0,00	0,00	0,00	0,00	0,00		0,00	0,00	0,00	0,00	0,00	0,00
XMg		0,27	0,33	0,32	0,38	0,30	0,27		0,50	0,55	0,51	0,60	0,52	0,52
Endmembers	Grs	0,28	0,24	0,23	0,15	0,20	0,17	Tri	0,06	0,06	0,07	0,07	0,00	0,06
	Prp	0,20	0,26	0,25	0,33	0,26	0,24	Prl	0,05	0,01	0,07	0,01	0,04	0,05
	Alm	0,50	0,48	0,50	0,50	0,51	0,56	Ms	0,63	0,32	0,56	0,62	0,43	0,63
	Sps	0,02	0,02	0,02	0,02	0,02	0,03	cel	0,12	0,26	0,13	0,20	0,29	0,12
								Pg	0,13	0,34	0,16	0,09	0,23	0,14

Mineral		Omph inclus.	Omph inclus.	Omph matrix	Omph matrix
Sample		L02b-gt21	E01-gt10	L02b-gt21	E01-s1
Analyse		14_4	56/1	18_2	36./2
SiO2		55,78	56,26	55,86	55,37
TiO2		0,09	0,11	0,09	0,39
Al2O3		13,14	13,94	9,13	13,61
FeO		6,67	6,30	7,86	6,59
MnO		0,00	0,05	0,08	0,01
MgO		6,56	5,67	9,12	5,78
CaO		11,13	10,15	12,97	10,45
Na2O		7,75	8,30	5,74	7,76
K2O		0,00	0,04	0,07	0,06
S		101,12	100,81	100,92	100,01
Structural Formulae					
Si		1,97	1,99	2,00	1,97
Ti		0,00	0,00	0,00	0,01
Al		0,55	0,58	0,39	0,57
Fetot		0,20	0,19	0,24	0,20
Mn		0,00	0,00	0,00	0,00
Mg		0,35	0,30	0,49	0,31
Ca		0,42	0,38	0,50	0,40
Na		0,53	0,57	0,40	0,54
K		0,00	0,00	0,00	0,00
Cr		0,00	0,00	0,00	0,00
XMg		0,64	0,61	0,67	0,61
Endmembers	acm	0,05	0,02	0,02	0,00
	jd	0,48	0,55	0,38	0,54
	hd	0,09	0,12	0,11	0,13
	di	0,29	0,25	0,38	0,25
	fe mg pyr	0,05	0,05	0,10	0,06
	Ca tsch	0,04	0,01	0,00	0,02

	amph inclus.	amph inclus.	amph matrix	amphi SZ
	H01-Gt13-II	H28-s2-II	H30-s2-II	H26a-s4-III
	79 / 1 .	120 / 1 .	147 / 1 .	5,00
	44,74	44,38	47,83	48,31
	0,29	0,29	0,39	0,34
	18,45	17,76	16,41	13,13
	9,22	7,75	7,64	5,72
	0,22	0,02	0,08	0,10
	14,29	13,38	13,39	15,62
	9,05	8,34	8,76	9,68
	2,21	4,60	4,55	3,06
	0,66	0,81	0,74	0,67
	99,13	97,34	99,78	96,63
	6,28	6,34	6,63	6,85
	0,03	0,03	0,04	0,04
	3,05	2,99	2,68	2,19
	1,08	0,93	0,89	0,68
	0,03	0,00	0,01	0,01
	2,99	2,85	2,77	3,30
	1,36	1,28	1,30	1,47
	0,60	1,27	1,22	0,84
	0,12	0,15	0,13	0,12
	0,02	0,00	0,00	0,00
	0,73	0,75	0,76	0,83

	czo	czo	czo
	C01-s1-II	C01-s4-II	C01-s4-II
	11	33	37
	38,89	40,00	39,49
	0,05	0,10	0,05
	31,03	30,83	31,74
	3,47	3,52	2,66
	0,04	0,01	0,00
	0,07	0,05	0,05
	23,38	23,43	24,17
	0,03	0,08	0,00
	0,00	0,00	0,00
	96,94	98,02	98,16
	6,05	6,14	6,04
	0,01	0,01	0,01
	5,68	5,58	5,72
	0,45	0,45	0,34
	0,00	0,00	0,00
	0,02	0,01	0,01
	3,89	3,85	3,96
	0,01	0,03	0,00
	0,00	0,00	0,00
	0,00	0,00	0,00
	0,03	0,02	0,03

The Fe^{3+} in garnet is assessed using Droop's (1987) method

rim Granulitic garnet rim, *matrix* not in contact with granulitic garnet, *Tri* trioctaedric mica, *prl* pyrophyllite and *fe mg pyr* orthopyroxene

sides) into core. The width of diffusional zoning is highly variable, even between two faces of a single garnet crystal, but is often as high as 50–100 μm. This reequilibration proceeds mainly through the substitution $FeMg^{-1}$, with minor enrichment in Ca. The most reequilibrated grt II has the composition $Alm_{57}Gr_{18}Py_{25}$ (Fig. 9).

Eclogitic garnet (grt III) The two distinct structures of eclogitic garnet, i.e. in the core of the fractures (grt III f) or in overgrowth on the rim of the granulitic garnet (grt III r), have compositions clustered in the same area of the triangle (Fig. 9), which is consistent with the evidence of eclogitic fracture merging into garnet overgrowth (Fig. 6). The grt III compositions are

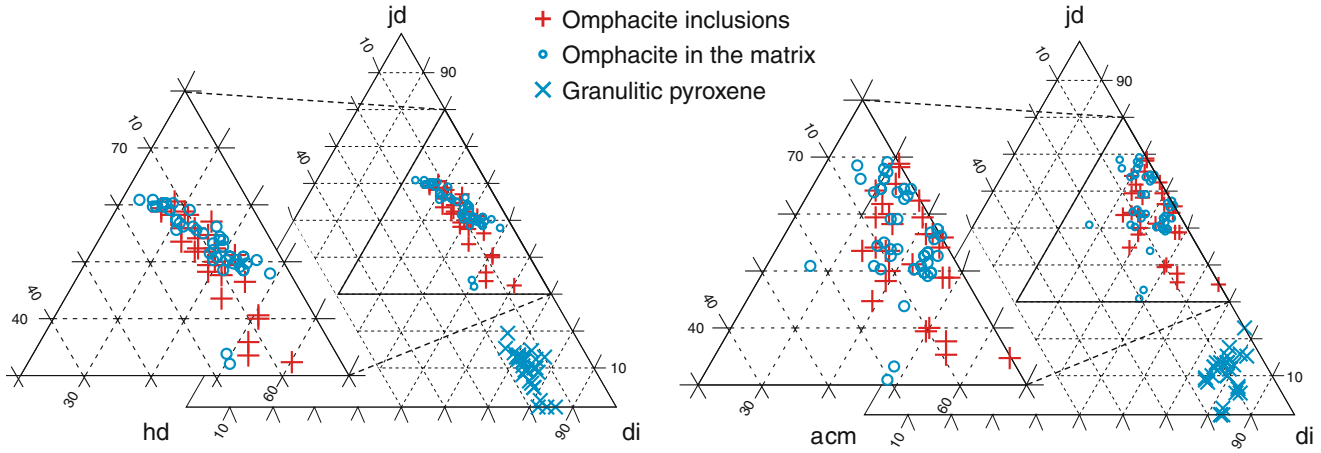

Fig. 7 Triangular decompositions of pyroxene compositions analysed with the electron microprobe. Three populations were distinguished: inherited granulitic pyroxene, eclogitic pyroxenes in fractures in garnet and eclogitic pyroxene out of garnet. The two eclogitic pyroxene populations plot on the same area of the triangles. *Jd* jadeite, *hd* hedenbergite, *di* diopside and *acm* acmite

relatively scattered with $0.48 < X_{alm} < 0.54$ and $0.23 < X_{gro} < 0.30$, but they are systematically richer in grossular than grt II. The almandine fraction is larger than in grt I, but slightly smaller than in grt II.

Grt II—III profiles In order to analyse the diffusion processes affecting the granulitic garnet, we have analysed concentration profiles perpendicular to eclogitic fractures, which run therefore in grt III f and in grt II. The chemical boundary between grt II and III f is sharp and consists mainly of a decrease in X_{alm} and X_{prp} and an increase in X_{gro}, from grt II to grt III (Fig. 10-1, 2). The amount of variation ranges from 1 to 5 % of endmember proportion depending on the profile. The chemical variation is qualitatively the same but is sharper on profiles 10—3 and 4, which run perpendicular to the grt II–III r boundary. The decrease in X_{alm} is ~5%, and the increase in X_{gro} is larger than 10% on profile 4.

While grt III is relatively homogeneous within each profile, the composition of grt II evolves between its outer boundary and the granulitic core that was not reequilibrated. This evolution is most manifested on profiles 3 and 4. Within grt II, the X_{alm} is maximum close to the grt II–III boundary, showing some kind of narrow plateau on profile 4, then decreases smoothly over ~100 μm to reach the X_{alm} of grt I. The X_{gro} of grt II is also maximum on its outermost border, then decreases sharply over ~20 μm to reach the X_{gro} of grt I.

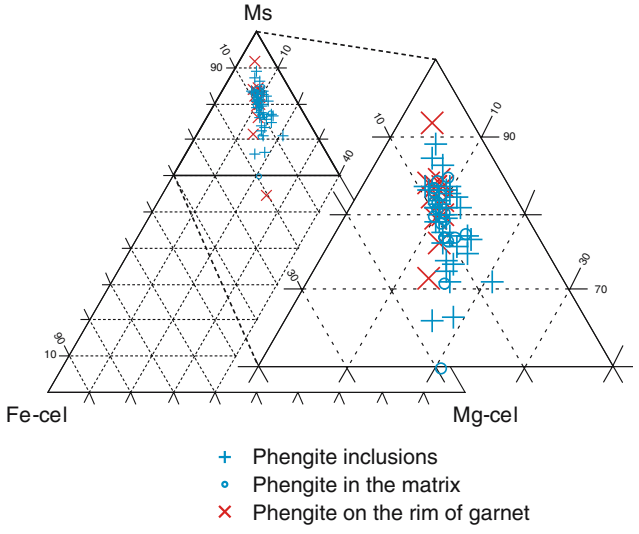

Fig. 8 Triangular decompositions of phengite compositions analysed with the microprobe. Three populations of eclogitic phengites were distinguished based on their position with respect to granulitic garnets: in fractures in garnets, in contact with the rim of the garnet and far from the garnets. All the phengite populations plot on the same area of the triangles. *Ms* muscovite and *cel* celadonite

Mineral relations within eclogitic fractures

The filling of the eclogitic fractures is made of discontinuous elongate inclusions of mainly omphacite and phengite and of grt III f between these inclusions. As a result these inclusions are in contact on their "long" side with grt II that makes the wall of the fracture, and on their "short" side with grt III f that filled in the fracture (Fig. 5). Profiles performed in inclusions show that most omphacite and phengite inclusions analysed are unzoned and therefore share sharp grain boundaries with both garnets grt II and III f (grt II–omphacite profiles are given later in Fig. 14). Thus, there is contact between *one* set of omphacite

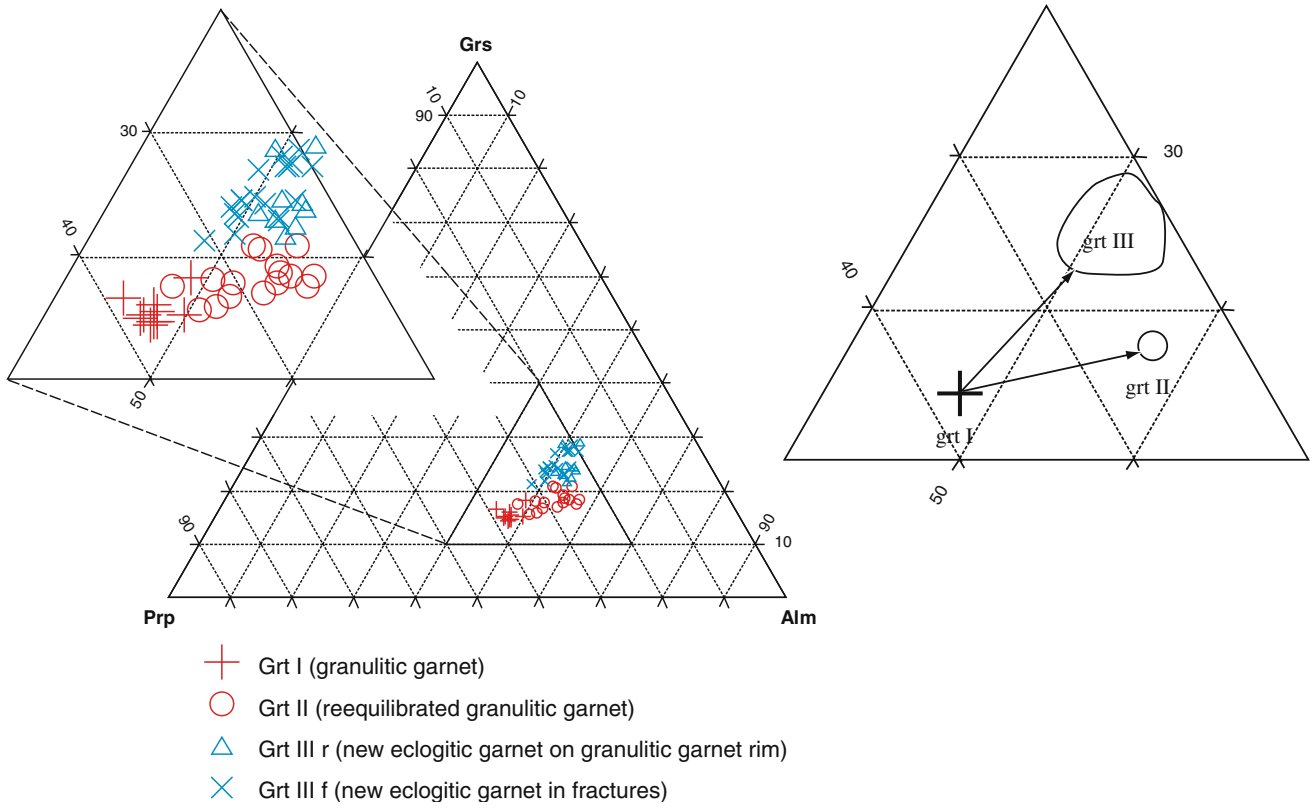

Fig. 9 Triangular decompositions of garnet compositions studied with the microprobe. The garnet populations were divided in four lots: preserved garnets (grt I), analysed in the core of inherited granulitic garnets; reequilibrated garnets (grt II), analysed near the rim of granulitic garnets; eclogitic garnet overgrowths (grt III r) and eclogitic garnet fracture filling (grt III f). The two latter eclogitic garnet compositions plot on the same area of the triangle. *Prp* pyrope, *alm* almandin and *grs* grossular. The sketch on the right shows the exchange vector leading to the equilibrium eclogitic composition (grt III), and the actual exchange vector that passes through the range of reequilibrated compositions (grt II)

and phengite compositions, and *two* sets of garnet with contrasted compositions.

Analysis of eclogite-facies metamorphism in fractures

Amphibolite-facies retrogression has affected eclogitised rocks, with a variable but on the average relatively low intensity. Although a large fraction of most eclogite-facies minerals in the matrix is preserved from retrograde reactions, rims are transformed to plagioclase + amphibole and plagioclase + pyroxene symplectites (Kühn 2002). On the other hand, retrogression is virtually absent from garnet fractures filling minerals, where contacts between adjacent high-pressure minerals are preserved. Eclogite-facies fractures are therefore the most appropriate settings to analyse the relations between grt II, grt III and HP minerals.

The veins are often a complex chemical system different from the whole rock system, due to significant ionic segregation (Dipple and Ferry 1992). This is not the case here, as omphacite, phengite and garnet have the same compositions in the core of matrix minerals and in eclogitic fractures filling minerals. The chemical system within fractures is therefore representative of bulk rock eclogite-facies transformation.

The problem of the existence of grt II

The close association within fractures of eclogite-facies minerals with two sets of garnets of different compositions is a clear evidence of disequilibrium texture. While grt II formed by diffusional reequilibration of inherited garnets, grt III both filled the eclogite-facies fractures along with other eclogite-facies minerals and grew from the rim of inherited garnets, including eclogite-facies minerals. This clear difference in the nature of the garnets, newly grown versus reequilibrated, leads to the conclusion that grt III is in equilibrium within eclogite-facies paragenesis, while grt II is a *partially* reequilibrated inherited garnet.

The second point to underline is the chronology between grt III crystallisation and grt II formation by

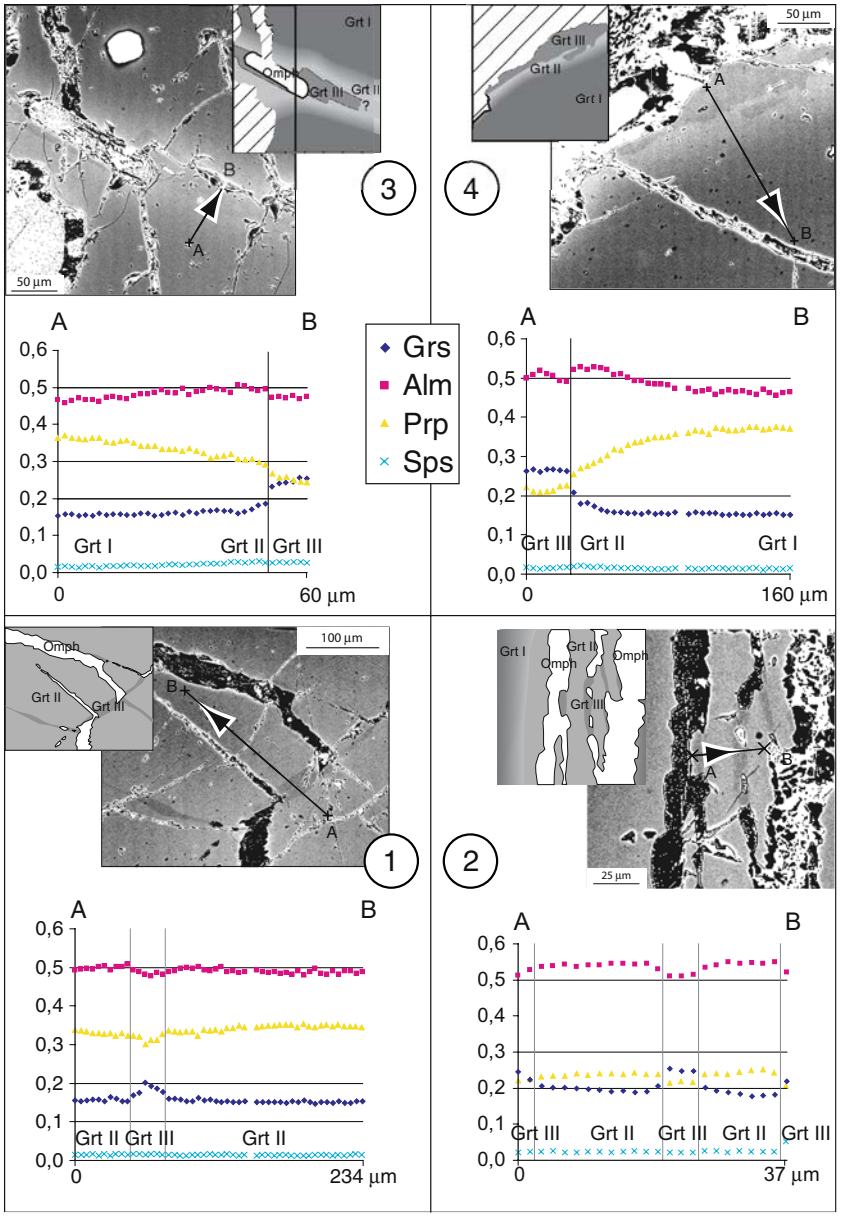

Fig. 10 Microprobe profiles within garnet running through the grt II–III boundary. The *top left* BSE photograph shows grt III located on the boundary of two granulitic garnets, the *top right one* eclogitic garnet overgrowth, the *bottom ones* eclogitic garnet filling eclogitic fractures within garnet. *Grs* garnet grossular and *Alm* almandine fractions. All profiles show a variable but sharp drop in grossular fraction and increase in almandine fraction from grt II into grt III. Within the granulitic garnet the reequilibration proceeds through a continuous increase in almandine fraction from core to rim, without change in Ca content

diffusion: (1) the almandine content of grt III, intermediate between granulitic garnet core (grt I) and reequilibrated rim compositions (grt II) and (2) the very little thickness (~5 µm) of grt III filling fractures, compared to the size of reequilibrated bands (~50 µm), leads to discard the hypothesis that grt II is formed by solid diffusion between eclogitic and granulitic garnet; the reequilibration of granulitic garnet must have occurred *prior* to eclogite-facies garnet crystallisation, leading to the following sequence of events (Fig. 11): fracturing of granulitic garnet, reequilibration of fracture rims and finally crystallisation of eclogite-facies minerals within the fractures. The timing of garnet fracturing is not precisely known, but as these fractures are much denser in eclogitised zones than in preserved granulite, it is likely that they are not inherited and formed early during eclogite-facies metamorphism.

The reequilibration of granulitic garnets is problematic, as it results mainly from $FeMg^{-1}$ exchange, while eclogite-facies garnets are significantly enriched in Ca. Two main reasons, examined hereafter, can account for the grt II formation: (1) grt II formed under different thermodynamic conditions, prior to the main crystallisation event in the fractures and in the matrix and/or (2) reequilibration processes are kinetically

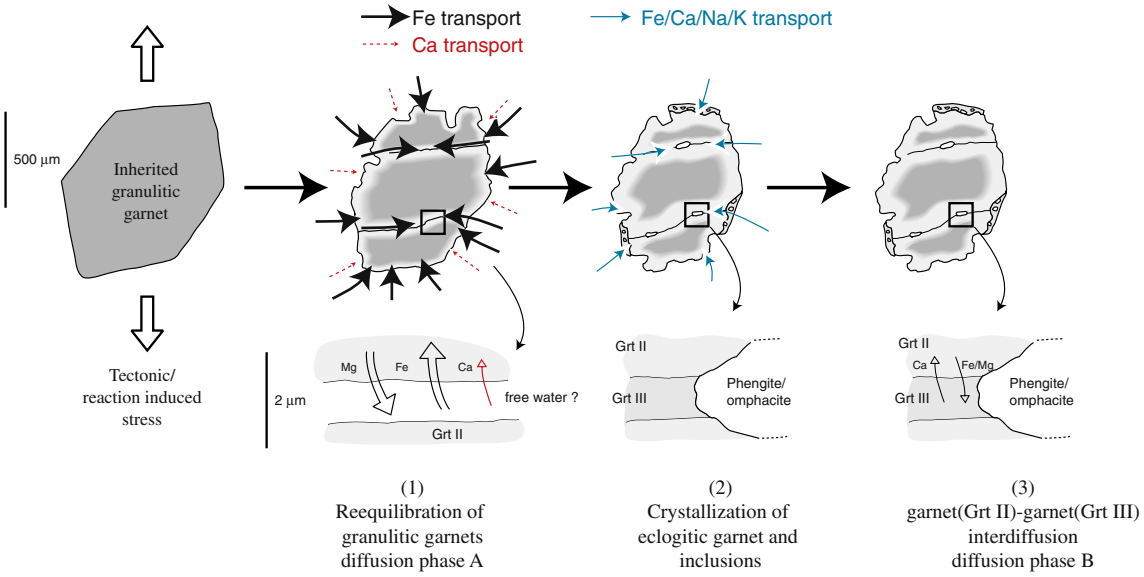

Fig. 11 Evolution model for garnet fracturing, diffusion and crystallisation within fractures during Caledonian eclogite-facies metamorphism. In the first stage (*1*), inherited granulite-facies garnets were fractured, in response to either tectonic or reaction-induced stresses, and reequilibrated by diffusion from their boundaries (diffusion phase A). In the second stage (*2*), crystallisation of omphacite, phengite and garnet (grt III) led to fracture annealing. There was little solid diffusion into the granulitic garnet during subsequent stage (*3*), as attested by the sharp compositional gradients across the grt II–III boundary (diffusion phase B)

controlled by the relative transport properties of Ca, Fe and Mg within garnet and in the matrix.

Thermobarometric analysis of equilibria in eclogitic fractures

In the following, *P–T* conditions are estimated for the main event of crystallisation of eclogite-facies minerals, including grt III. These estimations are used as mean conditions to build pseudosections, which explore whether variations in P, T conditions, reacting bulk rock compositions or water activity could be responsible for grt II formation.

P–T determinations

The eclogite-facies *P–T* conditions were determined with the software Thermocalc v3.1 (Holland and Powell 1990, 1998; Powell and Holland 1988), using triplets omphacite–phengite–grt III (minerals compositions microprobe analyses in Table 2). Only very few granulitic garnets have fractures containing inclusions of both phengite and omphacite. As a result, most of the estimations were carried out with either the phengite or the omphacite of the triplet taken not in the fracture but in the vicinity of the garnet analysed.

In the system H_2O–Na_2O–CaO–MgO–FeO–Fe_2O_3–Al_2O_3–SiO_2, with the phase components of garnet (grs–prp–alm), clinopyroxene (hd–di–jd), white mica (pg–cel–fcel–ms), quartz and H_2O, there are 12 – 8 = 4 independent reactions. A relevant set of reactions can be summarised as follows: Fe^{2+}–Mg^{2+} exchange between garnet, white mica and clinopyroxene (two independent reactions), the phengitic substitution Al^{-1} $Al^{-1}SiMg$, one reaction involving the Na-bearing phases (jadeite and paragonite) on each side. It is worth noting that this method uses only phases *actually* in equilibrium at eclogite-facies conditions, and therefore do not rely on the equilibrium albite → jadeite + quartz, which was used in several previous thermobarometric estimations (Austrheim and Griffin 1985; Mattey et al. 1994), although albite is absent from the eclogite-facies paragenesis.

The average of the *P–T* conditions on the 18 triplets analysed is 20.5 kbars and 718°C with grt III (Fig. 12). Both results are close to the conditions determined by Austrheim and Griffin (1985): 16–19 kbars and 700–800°C, (Jamtveit et al. 1990), >19 kbars and 700–750°C (Mattey et al. 1994) and 17 kbars and 700°C.

The uncertainty ellipse is enclosed in a rectangle of size $2\sigma_P \times 2\sigma T$, where σ_P and σ_T are uncertainties on P and T, respectively. The average $\overline{\sigma}_P$ over the 18 triplets is 3.5 kbars, while the average $\overline{\sigma}_T$ over the 18 triplets is 80°C.

Table 2 Electron microprobe analysis of triplets omphacite–garnet–phengite and corresponding equilibrium *P–T* conditions estimated with THERMOCALC

Mineral	Grt	Ms	Cpx	Grt	Ms	Cpx	Grt	Ms	Cpx
Sample	C01-Gt24-6	C01-gt24-V	C01-gt24-V	L02-Gt5-7	L02-Gt5-7	L02-Gt5-7	C01-gt7-V	C01-gt7-V	C01-gt7-V
Analyse	5/22	84/1	88/1	41/1	42/1	37/1	58/1	63/1	60/1
SiO_2	37.34	48.617	55.151	39.084	47.027	55.06	39.073	46.837	55.358
TiO_2	0.088	0.805	0.171	0.012	0.667	0.074	0.108	0.678	0.149
Al_2O_3	21.271	30.265	13.736	22.182	32.153	12.788	21.505	31.058	14.926
FeO	23.962	3.194	7.066	23.965	2.358	6.016	24.866	3.676	6.609
MnO	0.946	0.039	0.061	0.958	– 0.004	0.05	0.93	– 0.008	0.085
MgO	5.321	2.008	5.716	7.875	2.305	6.769	5.466	1.733	5.238
CaO	9.598	0.066	9.794	7.564	0.007	11.15	9.934	0.05	9.553
Na_2O	0.037	1.124	8.93	0.041	1.488	7.693	0.075	1.08	9.286
K_2O	– 0.009	7.893	– 0.021	0.004	9.074	– 0.005	– 0.006	7.872	– 0.009
Sum	98.554	94.011	100.604	101.685	95.075	99.595	101.951	92.976	101.195
	P (kbars)	23.5		*P* (kbars)	19		*P* (kbars)	23	
	ΔP (kbars)	3		ΔP (kbars)	3.1		ΔP (kbars)	4	
	T (°C)	635		*T* (°C)	769		*T* (°C)	705	
	ΔT (°C)	66		ΔT (°C)	72		ΔT (°C)	94	

PF is the volatil content

P–T pseudosections

Principle

P–T determination methods use actual mineral compositions and activity models, and compute independent reactions curves by zeroing Gibbs reaction energies $\Delta_r G$'s. The principle underlying pseudosections is the minimisation, for given *P–T* conditions, of the Gibbs energy (*G*) of the chemical system of interest, which is included but not necessarily equal to the bulk rock. The computation of this minimum, using software Thermocalc v3.1 (Holland and Powell 1990, 1998; Powell and Holland 1988) and input of system composition as well as relevant mineral activities (see Appendix for the latter), enables the determination of mineral modes and compositions.

Although the observed textures are characterised by some disequilibrium, as two generations of garnets are coexisting, pseudosections are the simplest way to study under which conditions of P, T, system composition, if they exist, grt II is stable. The much more precise forward modelling of the sample's prograde evolution is not possible, as we do not know in which order and with which proportions granulite-facies minerals got progressively involved in the eclogite-facies reactions.

The petrogenetic grids are built up by comparing the minimum value of *G* for all the assemblages with a variance ≥ 0 formed of a combination of minerals among the list muscovite–amphibole–paragonite–omphacite–garnet–orthopyroxene–epidote–quartz–kyanite–H2O. In the following, mineral assemblages are named

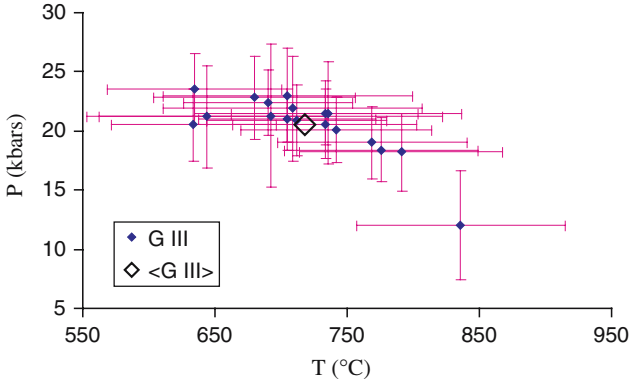

Fig. 12 *P–T* estimations performed with Thermocalc, using omphacite–phengite–garnet triplets (characteristic triplets are given in Table 3). Note that garnets used for these estimations are garnets grown at eclogite-facies conditions (grt III). In each triplet, either omphacite or phengite was an inclusion in an annealed eclogitic fracture through garnet. < *GIII* > refers to the average of *P–T* estimations made with grt III

after the missing minerals: [A, B] corresponds to an assemblage where all the minerals of the list above are present except A and B.

Whole rock analyses

The sample studied (C01) was collected in a little-transformed area, in dm-wide eclogitised band flanking both sides of a macroscopic fracture cutting through untransformed granulite. This sample was almost completely eclogitised, the only remnants of the granulite facies assemblage being granulitic garnets partially reequilibrated on their boundaries. grt III is present as overgrowths on granulitic garnet rims as well as vein infills. Locally, amphibolite facies symplectite overprinted eclogite-facies minerals. Whole rock analysis was performed in the ''Service d'Analyses des Roches et des Mineraux'' of the ''Centre de Recherches Petrographiques et Geochimiques'' in Vandoeuvre Les Nancy (see analysis of C01 on Table 3, plus, for the sake of reproductibility, the analysis of E01 and L02, sampled in another eclogitic bands, in the vicinity of C01).

Pseudosection construction requires the knowledge of the whole rock composition *at eclogite facies conditions*, but chemical analyses of the present sample incorporate all possible subsequent chemical variations associated with exhumation. The comparison of close samples of untransformed, strongly eclogitised and amphibolitised granulite specimen by Kühn (2002) demonstrates that the Caledonian metamorphism is isochemical at hand scale with respect to trace and major elements. The analyses of major elements carried out here are therefore relevant for the in situ eclogite facies whole rock composition.

We did not determine Fe^{3+} content, but we relied on the analyses of Kühn (2002) which states that the $\frac{FeO}{(FeO+Fe_2O_3)}$ ratio decreases from around 0.76 during granulite-facies conditions to values between 0.58 and 0.62 during eclogite-facies conditions, due to a change in oxydising conditions. We therefore used a value of 0.6.

Parameter variations

We have considered the variations in three independent parameters, in order to account for the absence of reequilibration in Ca of grt II: (1) *P–T* conditions, (2) fluid composition (water activity and amount of water available) and (3) composition of the reacting system.

Nature of the fluid On the basis of thermobarometric modelling and dihedral angle considerations respectively, Jamtveit et al. (1990) and Mattey et al. (1994) have reached the conclusion that eclogite-facies fluid is H_2O rich. The direct analysis of fluid inclusions in omphacite, although hampered by possible retrograde reactions between fluid inclusions and host minerals, confirmed that eclogitic facies fluids are saline brines, containing little CO_2 (between 2 and 12 mol.%) (Svensen et al. 1999). The variable brine salinity (Svensen et al. 2001) and extreme Pb fractionation (Svensen et al. 1999) attest to the consumption of H_2O by eclogite-facies reactions, leading to a decrease in water activity. In the transitional zones between granulite and eclogite, where little fluid was introduced during eclogite-facies metamorphism, such a decrease in water activity is evidenced by increased incorporation of Cl in amphiboles and the formation of different paragenesis in microcracks (Kühn 2002). The same kind of water activity decrease is likely to have occurred in the early stages of water introduction, even very near the macroscopic fracture, when fluid was consumed at the same time as it diffused from the fracture.

The H_2O content of C01 was estimated by loss on ignition (LOI). The present quantity of water is not necessarily the quantity that was actually present in the rock under eclogite facies conditions. The volatile content is indeed larger in the amphibolites than in the eclogites (Kühn 2002). The sample C01 shows the centimetre-scale areas of amphibolite-facies symplectites, but on the outcrop scale these samples are not in the vicinity of any of the amphibolitic decameter-sized fractures that enabled fluid input after eclogite-facies metamorphism. We assume therefore that amphibolitisation reactions used the stock of water already present in the samples and that no hydration was associated with this late metamorphic phase. As a result the present and the eclogite-facies water

Table 3 Chemical analyses of samples C01 (used in pseudosections), E01 and L02, all showing granulitic garnets fractures filled with grt III f, omphacite and phengite

Sample ref	SiO_2	Al_2O_3	Fe_2O_3	MnO	MgO	CaO	Na_2O	K_2O	TiO_2	P_2O_5	PF	Total
C01	52.07	18.71	8.7	0.14	5.25	8.27	5.15	0.93	0.43	<LD	0.42	100.07
E01	51.57	19.02	9.21	0.14	5.09	8.39	4.75	1.09	0.5	<LD	0.44	100.2
L02	52.57	19.53	8.34	0.13	5.09	8.7	3.95	0.99	0.47	<LD	0.26	100.03

content are considered as equal. Nevertheless, as water was progressively introduced from an external source (macroscopic fractures) during eclogite-facies metamorphism, this amount of water must be considered as a *maximum*, corresponding to late stages of eclogite-facies transformation, when water was abundant enough for the whole sample to react. The water available in early stages of eclogitisation may have been much scarcer.

As a result we set up two end-member cases: (a) pure H_2O fluid (water activity equal to 1), water amount equal to total LOI H_2O, corresponding to the final stages of eclogitisation, when all water was available and (b) saline brine (water activity reduced to 0.5) and water amount not constrained, but less than total LOI H_2O, corresponding to early metamorphic stages.

Reacting system The chemical system that tends to minimise its G under given P–T conditions is not necessarily the whole rock. The preservation of granulitic garnets with granulitic compositions (grt I) even in the most transformed samples is actually evident that the core of these garnets never reacted during the whole Caledonian history. As a consequence, this unreacting fraction ($V_{\text{unreacting}}$) must be subtracted from the whole rock analysis (V_{total}) to determine the correct chemical system ($V_{\text{reacting}} = V_{\text{total}} - V_{\text{unreacting}}$). The unreacting fraction is in our case the volume of grt I, which is equal to the volume of granulitic garnet minus its reequilibrated fraction ($V_{\text{unreacting}} = V_{\text{gran.garnet}} \times f_{\text{unreacting}}$). The proportion of granulitic garnet was determined optically from its 2D density on a thin section ($\sim 3 \times 4.5$ *cm*), and is equal to 13% for C01. The fraction of granulitic garnet not reequilibrated is highly variable from one garnet to another, but 100 μm can be considered as a characteristic width of reequilibrated rims, for garnets whose mean radius is ~500 μm. In this case, for spherical garnets, $f_{\text{unreacting}} = \sim 50\%$. This estimate is a *minimum*, corresponding to final stages of metamorphism, while in initial stages, inherited granulitic garnets are not involved in reactions and $f_{\text{unreacting}} = \sim 100\%$. As variable fractioning of elements in garnets, depending on the size of reequilibrated rims, may strongly affect the equilibrium assemblages (Florence and Spear 1995; Konrad-Schmolke et al. 2005; Marmo et al. 2002; Stüwe 1997), we have build up pseudosections in these three endmembers cases: $f_{\text{unreacting}} = 100$, 75 and 50%.

Results

Eclogite-facies equilibrium P–T conditions (20.5 kbars, 718°C), plotted as a star (Fig. 13), are for all studied conditions within the field [amph, opx, epid], but for $a_{H2O} = 1$ and $f_{\text{unr}} = 100\%$, where they lie within the field [amph, opx]. The most appropriate conditions for forming assemblages in agreement with eclogite-facies minerals analysed in natural samples are $f_{\text{unreacting}} = 50\%$, irrespective of water activity. The computed conditions are consistent with the fact that main eclogite-facies minerals crystallised *after* reequilibration of granulitic garnets (Fig. 11), therefore $f_{\text{unreacting}}$ is minimum. The variations in water activity and amount have a large influence on the field boundaries, but very slightly affect the equilibrium compositions within a given field for fixed P–T conditions.

For $f_{\text{unreacting}} = 50\%$, omphacite is the dominant mineral in the computed modes. It can be decomposed as 0.51 jadeite, 0.30 diopside, 0.11 hedenbergite and 0.08 acmite. The jadeitic substitution between jadeite and diopside ($NaAlCa^{-1}Mg^{-1}$) is therefore equal to 62%, which is in the range encountered in the analysed omphacites (50–70% jadeitic substitution, see Mineral chemistry). The second index mineral is phengite, and the computed stoechiometric silicium content is 3.26 Si atoms per phengite. This value is very close to the 3.15–3.25 range analysed in phengites. The computed garnet composition ($X_{\text{alm}} = 0.52$, $X_{\text{gro}} = 0.285$) is also in agreement with grt III f compositions ($0.48 < X_{\text{alm}} < 0.54$ and $0.23 < X_{\text{gro}} < 0.30$).

If the assemblage described above attests to the validity of activity models and pseudosections computed, the main objective is to analyse whether reequilibration of granulitic garnets may have occurred *at equilibrium*, under conditions different from the main crystallisation event. To study the variations in the equilibrium garnet compositions within various fields, the isopleths of almandine and grossular fractions in garnet are drawn. Whatever field and conditions are considered, grossular fraction is >26%; furthermore, in conditions corresponding to early stages of the reaction, when granulitic garnets have not yet been involved in reactions ($f_{\text{unreacting}} = 100\%$), grossular fractions are even much higher, >35% over the whole P–T grid, completely disagreeing with the low grossular content (<20%) of grt II. It should also be noted that whatever conditions of water activity and reacting fraction are considered, an average prograde evolution leading to the calculated peak P and T, which is thought to correspond to the settings of grt II formation (see Discussion), is always associated with an *increase* in the grossular content, irrespective of its absolute value.

In conclusion, pseudosections yielded, therefore, realistic mineral assemblage for the main crystallisation event, but were unable to account for the

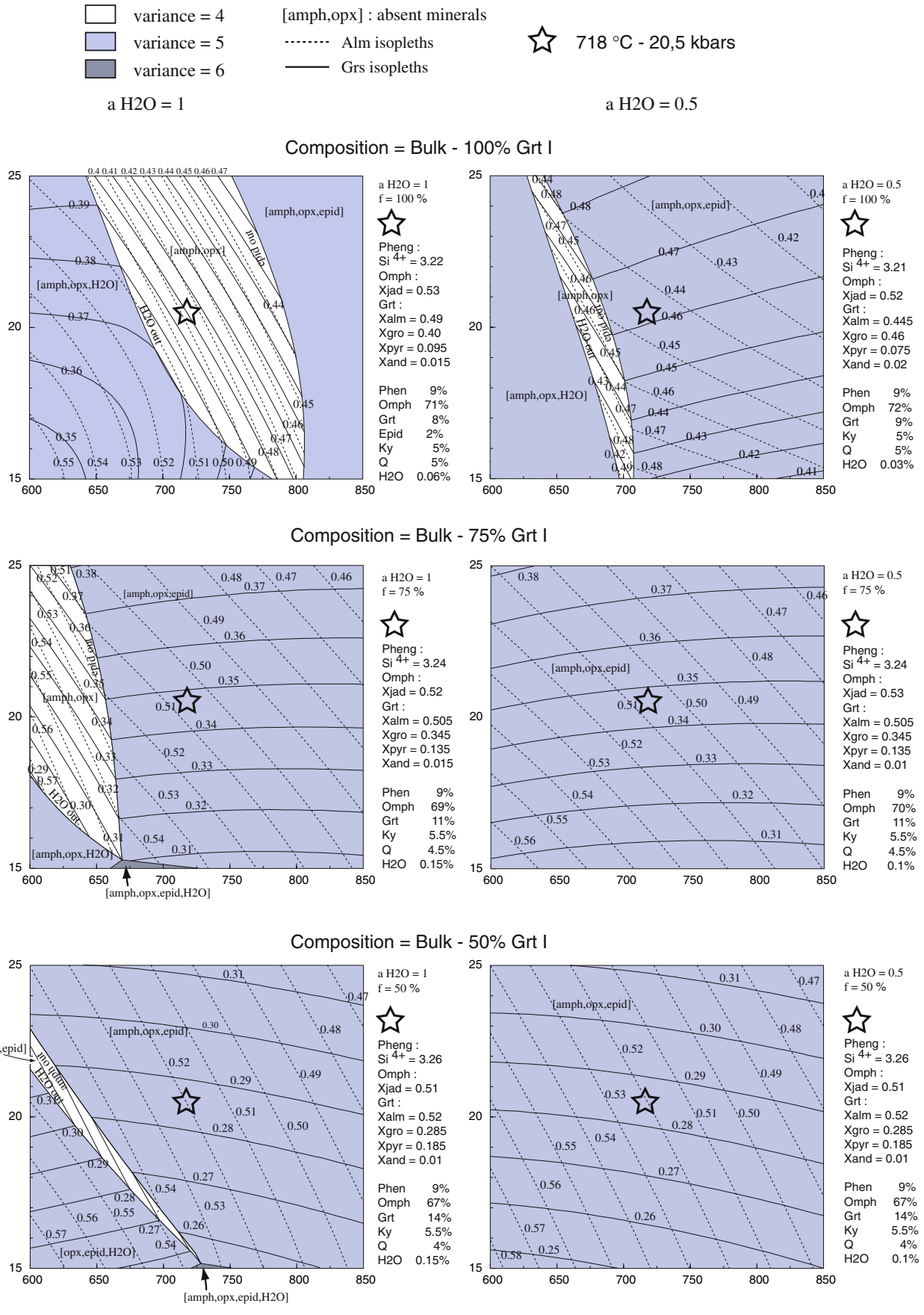
variance = 4
variance = 5
variance = 6
[amph,opx] : absent minerals
Alm isopleths
Grs isopleths
718 °C - 20,5 kbars
a H2O = 1
a H2O = 0.5
Composition = Bulk - 100% Grt I
Composition = Bulk - 75% Grt I
Composition = Bulk - 50% Grt I
[amph,opx,epid]
[amph,opx]
[amph,opx,H2O]
[amph,opx,epid,H2O]
[opx,epid]
[opx,epid,H2O]
no epid
epid out
H2O out
a H2O = 1
f = 100 %
Pheng :
Si 4+ = 3.22
Omph :
Xjad = 0.53
Grt :
Xalm = 0.49
Xgro = 0.40
Xpyr = 0.095
Xand = 0.015
Phen 9%
Omph 71%
Grt 8%
Epid 2%
Ky 5%
Q 5%
H2O 0.06%
a H2O = 0.5
f = 100 %
Pheng :
Si 4+ = 3.21
Omph :
Xjad = 0.52
Grt :
Xalm = 0.445
Xgro = 0.46
Xpyr = 0.075
Xand = 0.02
Phen 9%
Omph 72%
Grt 9%
Ky 5%
Q 5%
H2O 0.03%
a H2O = 1
f = 75 %
Pheng :
Si 4+ = 3.24
Omph :
Xjad = 0.52
Grt :
Xalm = 0.505
Xgro = 0.345
Xpyr = 0.135
Xand = 0.015
Phen 9%
Omph 69%
Grt 11%
Ky 5.5%
Q 4.5%
H2O 0.15%
a H2O = 0.5
f = 75 %
Pheng :
Si 4+ = 3.24
Omph :
Xjad = 0.53
Grt :
Xalm = 0.505
Xgro = 0.345
Xpyr = 0.135
Xand = 0.01
Phen 9%
Omph 70%
Grt 11%
Ky 5.5%
Q 4.5%
H2O 0.1%
a H2O = 1
f = 50 %
Pheng :
Si 4+ = 3.26
Omph :
Xjad = 0.51
Grt :
Xalm = 0.52
Xgro = 0.285
Xpyr = 0.185
Xand = 0.01
Phen 9%
Omph 67%
Grt 14%
Ky 5.5%
Q 4%
H2O 0.15%
a H2O = 0.5
f = 50 %
Pheng :
Si 4+ = 3.26
Omph :
Xjad = 0.51
Grt :
Xalm = 0.52
Xgro = 0.285
Xpyr = 0.185
Xand = 0.01
Phen 9%
Omph 67%
Grt 14%
Ky 5.5%
Q 4%
H2O 0.1%

◀ **Fig. 13** Pseudosections built with a bulk composition equal to $C_{C01} - fC_{grt\ I}$, where C_{C01} is the bulk composition of C01, $C_{grt\ I}$ is the composition of the granulitic garnet times its massic proportion and f is the proportion of inherited garnet that remained unreacted during eclogite-facies metamorphism. Each field is labelled after the set of minerals absent in the equilibrium assemblage. A line separating two fields with different variances is named after the mineral that disappears between the two assemblages. *Solid lines* are grossular isopleths and *dashed lines* almandine isopleths. On the right, minerals' modes and compositions were computed at the *P–T* conditions assessed with eclogite-facies paragenesis (*black star*). Pseudosections in the right column are built with $a_{H2O} = 0.5$, those in the left column with $a_{H2O} = 1$. Values of f decrease from top to bottom row with values of 100, 75 and 50%. Computed equilibrium assemblages formed at 720°C and 20.5 kbars for $f = 50\%$ are in good agreement with eclogite paragenesis crystallised in garnet fractures. On the other hand, whatever conditions of water activity, reacting system composition, pressure or temperature are considered, computed equilibrium garnet compositions are notably richer in grossular than reequilibrated granulitic garnets

reequilibration of granulitic garnets. Therefore, even if it is only a negative proof, this study strongly supports the hypothesis that garnet reequilibration under eclogite-facies, leading to grt II compositions, is not thermodynamically but kinetically controlled.

Discussion

Reequilibration-limiting processes

Granulitic garnet reequilibration is controlled by several elementary processes (Dohmen and Chakraborty 2003), and processes external to garnets, such as slow intergranular diffusion of Ca, as well as internal ones, such as slow intra-granular diffusion of Ca within garnet, can both be responsible for the lack of reequilibration in Ca of granulitic garnets.

There are many experimental studies aiming at characterising diffusion properties within garnets (Chakraborty and Ganguly 1992; Chakraborty and Rubie 1996; Cygan and Lasaga 1985; Elphick et al. 1985; Ganguly et al. 1998; Loomis et al. 1985). However, their applicability is restricted to the range of garnet compositions used and as far as we know, only Ganguly et al.'s (1998) experimental ferro-magnesian garnets are reasonably close to the granulitic garnets of our study. These authors retrieved garnet self-diffusion coefficients such as $D^*_{Mg} > D^*_{Ca} \simeq D^*_{Fe}$. Such self-diffusion coefficients are not sufficient to assert that diffusional reequilibration in Fe and Ca should proceed at the same rate, as the flux of a single element is defined by a complex expression integrating the self-diffusion diffusion of *all* diffusing elements, as well as concentration gradients, but they still show that Fe and Ca have not a significantly different diffusional behaviour. In addition to these experimental data, analysis of zoning profiles in natural garnets (Carlson 2002, 2006) also leads to the conclusion that $D^*_{Ca} \simeq D^*_{Fe}$ in garnets, similarly to our study.

An additional explanation to the lacking reequilibration in Ca of the granulitic garnets is the possible inefficiency of Ca intergranular diffusion with respect to Fe and Mg. The study of diffusion-controlled garnet growth (Chernoff and Carlson 1997, 1999) showed that Mn, Mg and Fe achieved chemical equilibrium at hand-scale, while Ca concentrations were strongly variable between garnets, denoting kinetically-controlled incorporation. The low intergranular diffusion rates of Ca compared to Fe and Mg deduced from these study and also from Carlson (2002), Lang and Gilotti (2001) and Spear and Daniel (2001) are a likely explanation for the lack of Ca reequilibration observed in the granulitic garnets we analysed.

Although our study does not enable to distinguish between slow intergranular and intra-garnet diffusion, it seems from the above analysis of literature data that the inefficiency of calcium transport between matrix and garnets is the dominant factor in the sluggish calcium transport.

Nevertheless, eclogite-facies grt III, growing after granulitic garnet reequilibration, is Ca-rich, unzoned and in equilibrium with other eclogite-facies minerals (see Pseudosection analysis). Grt III is therefore a strong evidence of Ca mobility and availability *during the main crystallisation event*. Therefore, if it is likely that slow Ca intergranular diffusion hampered granulitic garnet reequilibration during an early metamorphic phase, we do not know what changes in the intergranular medium have resulted in much higher transport rates during the main metamorphic event, when grossular-rich grt III crystallised.

Reequilibration path

The slow Ca intergranular diffusion kinetics restricted garnet reequilibration to Fe^{2+}–Mg exchange, as observed in our sample. Along this vector, granulitic garnet reequilibration, occurring in an early phase of eclogite-facies metamorphism, was controlled by Fe–Mg partitioning with adjacent clinopyroxenes. The composition of the clinopyroxene exchanging Fe and Mg with the granulitic garnet is not known and may differ from the large inherited granulite-facies clinopyroxenes. In fact, in only slightly eclogitised areas, although the cores of these large clinopyroxenes preserve a granulitic composition, their rims are transformed into tiny clinopyroxenes with a large jadeitic

component, much similar to the ones later crystallising within the fractures (Raimbourg 2005). We assume therefore that the Fe–Mg partitioning, which drives the diffusional reequilibration of the granulitic garnet, is done with a pyroxene whose composition is similar to the eclogite-facies omphacite and not with inherited granulitic pyroxene. In the following, we analyse the equilibrium between both grt II and III formed within the same fractured garnet and omphacite compositions from an inclusion of this garnet. We emphasise that granulitic garnet did not reequilibrate with this actual omphacite grain, which crystallised later (Fig. 11), but rather that this omphacite has a composition similar to the pyroxenes in the neighbourhood of the garnet with which it reequilibrated.

Profiles running perpendicular to fractures, within fracture-filling omphacite and adjacent grt II (Fig. 14), show the relative homogeneity of omphacite compositions from core to the rim. From this range omphacite compositions (shaded surface), we have computed garnet compositions in equilibrium at 718°C and 20.5 kbars as to Fe–Mg partitioning, according to the following clinopyroxene–garnet geothermometer (Krogh Ravna 2000b):

$$T(\mathrm{K}) = \frac{3.104X_{\mathrm{Ca}}^{\mathrm{grt}} + 3.030 + 10.86\,P(\mathrm{kb})}{\ln K_D + 1.9034}$$

with $K_D = \frac{(\mathrm{Fe}^{2+}/\mathrm{Mg}^{2+})^{\mathrm{grt}}}{(\mathrm{Fe}^{2+}/\mathrm{Mg}^{2+})^{\mathrm{Cpx}}}$

For given T and omphacite composition, an increase in $X_{\mathrm{Ca}}^{\mathrm{grt}}$ at equilibrium is offset by an increase in K_D, therefore by a decrease in $x_{\mathrm{Mg}}^{\mathrm{grt}}$.

In conclusion, Fe–Mg partitioning between both grt II and III and omphacite is equal to equilibrium values computed with Krogh Ravna's (2000b) relation at 718°C and 20.5 kbars. Furthermore, $x_{\mathrm{Mg}}^{\mathrm{grt}}$ differences between grt II and III, for equilibrium with the same omphacite composition, are in qualitative agreement with the $X_{\mathrm{Ca}}^{\mathrm{grt}}$ dependence of Ellis and Green's (1979) relation.

Although granulitic garnet reequilibration in Ca was hampered by a slow intergranular diffusivity, reequilibration by Fe–Mg exchange is carried thoroughly up to Fe–Mg partitioning equilibrium with omphacite, with equilibrium $x_{\mathrm{Mg}}^{\mathrm{grt\ II}}$ different from $x_{\mathrm{Mg}}^{\mathrm{grt\ III}}$ due to lower grossular content. We propose therefore that, although grt II formed *before* grt III crystallisation, they are both at Fe–Mg partitioning equilibrium with the same omphacite for the same P–T conditions, which implies that (1) grt II is also an *eclogite-facies garnet* and not a garnet inherited from a previous metamorphic event and (2) omphacite started forming early during the eclogite-facies metamorphic event and kept a relatively constant composition throughout it.

$$T(^{\circ}\mathrm{C}) = \frac{\left[\begin{array}{l} 1.939.9 + 3.270X_{\mathrm{Ca}}^{\mathrm{grt}} - 1.396\,(X_{\mathrm{Ca}}^{\mathrm{grt}})^2 + 3.319\,X_{\mathrm{Mn}}^{\mathrm{grt}} - 3.535\,(X_{\mathrm{Mn}}^{\mathrm{grt}})^2 \\ + 1.105\,X_{\mathrm{Mg\#}}^{\mathrm{grt}} - 3.561(X_{\mathrm{Mg\#}}^{\mathrm{grt}})^2 + 2.324(X_{\mathrm{Mg\#}}^{\mathrm{grt}})^3 + 169.4P(\mathrm{GPa}) \end{array}\right]}{\ln K_D + 1.223} - 273$$

where $X_{\mathrm{Mg\#}}^{\mathrm{grt}} = \frac{\mathrm{Mg}}{\mathrm{Fe}^{2+}+\mathrm{Mg}}$, $X_{\mathrm{Ca}}^{\mathrm{grt}} = \frac{\mathrm{Ca}}{\mathrm{Ca}+\mathrm{Fe}^{2+}+\mathrm{Mn}+\mathrm{Mg}}$, $X_{\mathrm{Mn}}^{\mathrm{grt}} = \frac{\mathrm{Mn}}{\mathrm{Ca}+\mathrm{Fe}^{2+}+\mathrm{Mn}+\mathrm{Mg}}$, and $K_D = \frac{(\mathrm{Fe}^{2+}/\mathrm{Mg}^{2+})^{\mathrm{grt}}}{(\mathrm{Fe}^{2+}/\mathrm{Mg}^{2+})^{\mathrm{Cpx}}} = \frac{x_{\mathrm{Mg}}^{\mathrm{Cpx}}}{x_{\mathrm{Mg}}^{\mathrm{grt}}}$.

In both profiles (Fig. 14), $x_{\mathrm{Mg}}^{\mathrm{grt}}$ ($x_{\mathrm{Mg}}^{\mathrm{grt}} = \frac{\mathrm{Mg}}{\mathrm{Fe}^{2+}}$ in garnet, note the difference with $X_{\mathrm{Mg\#}}^{\mathrm{grt}}$ and $X_{\mathrm{Mg}}^{\mathrm{grt}}$) decreases sharply from the unreequilibrated core to the zone next to omphacite, where Fe–Mg partitioning with omphacite is at equilibrium.

Similar calculations performed in the same granulitic garnets with grt III (point C) and the same omphacite compositions show that although grt III compositions are much different from grt II, equilibrium partitioning with omphacite is also achieved.

Although grt II and III have very different compositions, they have relatively close $x_{\mathrm{Mg}}^{\mathrm{grt}}$, which are both at equilibrium with adjacent omphacite. Their little but quite systematic difference ($x_{\mathrm{Mg}}^{\mathrm{grt\ III}}$ is slightly smaller than $x_{\mathrm{Mg}}^{\mathrm{grt\ II}}$) is well accounted for by the $x_{\mathrm{Ca}}^{\mathrm{grt}}$ dependence of the clinopyroxene-garnet Fe–Mg partition relation (Ellis and Green 1979):

Existence of two eclogite-facies phases

The observation of two distinct garnet generations (grt II and III) enables us to divide eclogite-facies metamorphism into two successive events. Textural (the close association between grt II and fractures, whose density is controlled by eclogitisation extent) as well as thermobarometric considerations (Fe–Mg partitioning between garnet and omphacite) demonstrate that the two metamorphic phases are closely related and occurred under similar metamorphic conditions. This scenario does not nevertheless provide any explanation for the division of eclogite-facies metamorphism into a first phase of granulitic garnet reequilibration followed

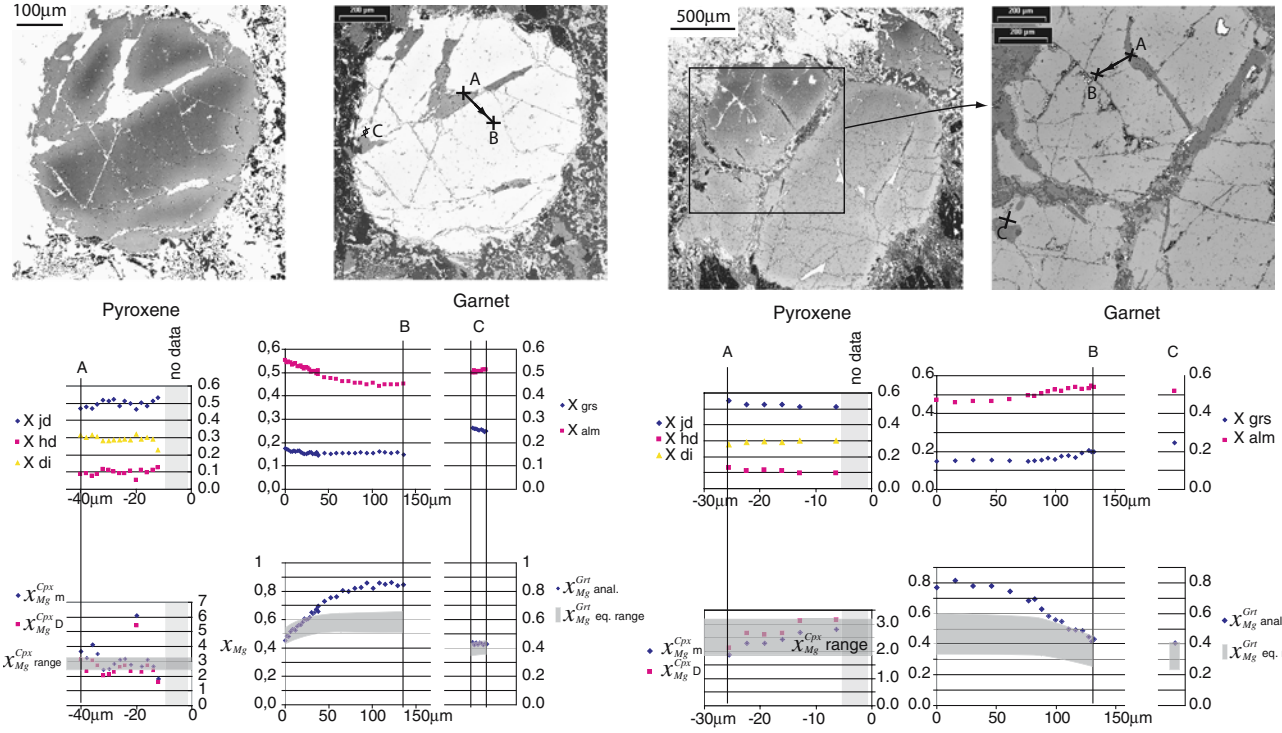

Fig. 14 *A–B* Electron microprobe profiles through omphacite and adjacent reequilibrated garnet (grt II). Distances in microns are measured from the boundary between omphacite and garnet. *C* Eclogite-facies garnet overgrowth (grt III) analysis, either as single point (*right*), or as profile along a segment (*left*). Upper profiles show Jd–Hd–Di and Grs–Alm fractions in omphacite and garnet, respectively. x_{Mg}^{Cpx} (*left lower profiles*) are computed either as $\frac{X_{Di}}{X_{Hd}}$ after the matrix decomposition of the pyroxene using the six endmembers Acm–Jd–Hd–Di–Fe/Mg_Px–CaTsch (x_{Mg}^{Cpx} m) or as $\frac{Mg}{Fe_{Tot}-Fe^{3+}}$, assessing Fe^{3+} using Droop's (1987) method (x_{Mg}^{Cpx} D). The range of x_{Mg}^{Cpx} values deduced is used as input in Krogh Ravna' (2000b) geothermometer, enabling to estimate the range of garnet's x_{Mg}^{grt} in equilibrium at 720°C and 20.5 kbars with analysed omphacite, as to Fe^{2+}–Mg partitioning. Although having very different compositions, both eclogite-facies garnet compositions (grt III–point C) and most reequilibrated granulitic garnet compositions (grt II–point B) are in equilibrium with omphacite, while x_{Mg}^{grt} in unreequilibrated cores is much above equilibrium values. Reequilibration of inherited garnets in terms of Fe^{2+}–Mg exchange is controlled by exchange with eclogite-facies omphacite

by a phase of eclogitic garnet crystallisation. In addition, cation mobility varied strongly between the two phases, enabling Ca transport within the eclogitic fractures during the second phase.

This transition may be explained by the evolution of the system fluid + minerals at equilibrium under changing *P–T* conditions. This mechanism was proposed for albite crystallisation during isothermal decompression (Jamieson and O'Beirne-Ryan 1991). The solutes' concentrations in equilibrium with a given mineral assemblage evolve as *P–T* conditions changes, leading to mineral crystallisation or dissolution. Unfortunately, experimental data on the behaviour of solutes in the fluid are restricted to a pressure range much lower than the eclogite-facies conditions (for example the software SUPCRT92 calculates solute concentrations up to 5 kbars; Johnson et al. 1992)), so this hypothesis cannot be tested. While the rock has already started eclogitising, a drastic change in *P–T evolution*, not necessarily associated to a large change in *P–T* conditions, could result in the inception of eclogitic garnet crystallisation. As the structural analysis by Raimbourg et al. (2005a) shows that the eclogite-facies deformation records the first steps of exhumation, eclogitisation reactions may have spanned both the end of the prograde and the start of the retrograde path, and the movement and *P–T* evolution reversal could have induced eclogitic garnets crystallisation.

P–T–t evolution of the unit

The temporal extent of the two eclogite-facies phases is strongly asymmetrical. The duration of the first phase is sufficient for the Fe^{2+} to penetrate by diffusion into granulitic garnet over a distance of the order of 50–100 µm. During the second phase, eclogitic garnet crystallised on the border of the reequilibrated granu-

litic garnet; in spite of their different compositions, little cation exchange occurred between grt II and III.

Phase A: granulitic garnet reequilibration

We have modelled granulitic garnet composition profiles perpendicular to a fracture (Fig. 15), resulting from diffusion from the fracture, similarly to Erambert and Austrheim (1993). Note that for the sake of accurate modelling, we have used a sample from a different location where Fe–Mg exchanges are larger than in those presented above. We considered diffusion in a semi-infinite plane, with concentrations at the surface held constant for $t \geq 0$. As seen from the profile, the absence of variations in Ca enables to reduce the problem to simple interdiffusion between Fe and Mg, the former being considered as the dependent cation. The solution to such a problem is given by Crank (1975) as:

$$X_{\mathrm{Mg}}(x) = X_{\mathrm{Mg}}^{\mathrm{ext}} + (X_{\mathrm{Mg}}^{\mathrm{int}} - X_{\mathrm{Mg}}^{\mathrm{ext}})\mathrm{erf}\left(\frac{x}{\sqrt{4D_{\mathrm{Fe-Mg}}t}}\right),$$

where the distance x is measured from the fracture, $X_{\mathrm{Mg}}^{\mathrm{ext}}$ the composition at the garnet surface, $X_{\mathrm{Mg}}^{\mathrm{int}}$ the composition in the unreequilibrated core and D_{Fe}–Mg the Fe–Mg interdiffusion coefficient. $X_{\mathrm{Mg}}^{\mathrm{int}}$ was assessed around 0.55 at several points in the garnet where the profile was carried out, while $X_{\mathrm{Mg}}^{\mathrm{ext}}$ was estimated around 0.34–0.35 in several highly fractured garnets of the same thin section showing reequilibrated zones with plateau composition. The interdiffusion coefficient D_{Fe}–Mg was assessed according to Barrer et al. (1963):

$$D_{\mathrm{Fe-Mg}} = \frac{D_{\mathrm{Fe}}^{*} D_{\mathrm{Mg}}^{*}}{X_{\mathrm{Fe}} D_{\mathrm{Fe}}^{*} + X_{\mathrm{Mg}} D_{\mathrm{Mg}}^{*}}$$

Self-diffusion coefficients derived from pyrope–almandine diffusion coupled by Ganguly et al. (1998) are the most appropriate for our diffusion problem:

$$D_{\mathrm{Fe}}^{*} = 3.5 \times 10^{-9} \exp \times \left(-\frac{274(\mathrm{kJ/mol}) + 5.6P(\mathrm{GPa})}{\mathrm{RT}} \times 10^{3}\right) \mathrm{m^2/s}$$

$$D_{\mathrm{Mg}}^{*} = 4.66 \times 10^{-9} \exp \times \left(-\frac{254(\mathrm{kJ/mol}) + 5.3P(\mathrm{GPa})}{\mathrm{RT}} \times 10^{3}\right) \mathrm{m^2/s}$$

The same coefficients were indeed used by Perchuk (2002) for his analysis of diffusion profiles in garnets from the same high-pressure unit as this study. To account for the evolution of the temperature during diffusion, we use not the peak metamorphic temperature $T_0 = 720°\mathrm{C}$ but rather a "characteristic temperature" defined as $T_c \approx 0.97T_0 \approx 700°\mathrm{C}$ (Chakraborty and Ganguly 1990, 1992). Depending on the garnet composition considered, corresponding either to rim or core, at 700°C and 20.5 kbars, interdiffusion coefficients are, respectively (Chakraborty and Ganguly 1992; Lasaga 1979):

$$D_{\mathrm{Fe-Mg}}^{\mathrm{rim}} = 4.28 \times 10^{-24}\,\mathrm{m^2/s}$$

$$D_{\mathrm{Fe-Mg}}^{\mathrm{core}} = 2.86 \times 10^{-24}\,\mathrm{m^2/s}$$

The time necessary to achieve the diffusion profiles (Fig. 15) is given approximately by $x_{1/2} = \sqrt{D_{\mathrm{Fe-Mg}}t}$, where $x_{1/2}$ is the penetration depth, i.e. the distance from the rim where the concentration is the average of rim and core composition. With $x_{1/2} = 33\ \mu\mathrm{m}$ and using the interdiffusion coefficients the two extreme values given above, the diffusion time at 700°C and 20.5 kbars is comprised between 8 and 12 Ma. Alternatively, using the diffusion coefficients from Carlson (2006) ($D_{\mathrm{Fe}}^{\mathrm{rim}}$ – Mg = 4.66×10^{-3} m^2/s and $D_{\mathrm{Fe}}^{\mathrm{core}}$ – Mg = 1.89×10^{-23} m^2/s) yielded a diffusion time range of 0.7–1.8 Ma, in good agreement with the 1–4 Ma time lapse assessed by Erambert and Austrheim (1993). A precise estimation of the temperature is crucial, as at 650°C, diffusion times increase by more than a factor of 5 (54–81 Ma with Ganguly et al. (1998) coefficients).

Phase B: grt II–III interdiffusion

After crystallisation of eclogitic garnet on the rims of inherited garnets, the difference in composition between both garnets led to a second phase B of diffusion. We assume that the crystallisation of eclogite-facies garnet overgrowths was instantaneous with respect to diffusion processes. The reequilibration between new and inherited garnets implies Ca flux out and Fe and Mg flux in for grt III, so it is a ternary diffusion problem. In addition, while eclogite-facies garnet composition is homogeneous at the start of phase B, granulitic garnets rim are strongly heterogeneous in Fe and Mg due to the reequilibration during phase A.

Following Chakraborty and Ganguly (1992), the ternary diffusion problem can be reduced to a pseudobinary problem, one cation being treated as a solute and the rest of the solution as a solvent. Ca was chosen

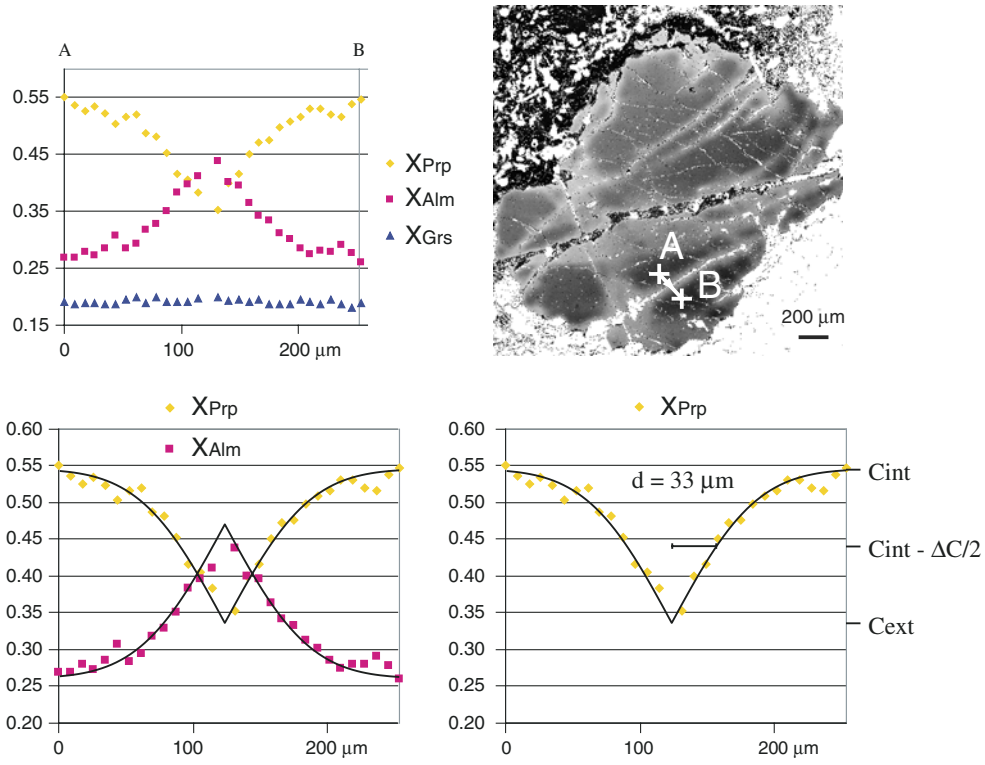

Fig. 15 Electron microprobe profiles across an eclogite-facies fracture, showing the penetrative reequilibration of inherited granulitic garnets by Fe^{2+}–Mg^{-1} exchange at constant X_{Ca}. Composition profiles are modelled as resulting from the diffusion within an infinite half-space, initially homogeneous ($C^{int}_{Mg} \approx 0.55$), from the fracture, where the composition is assumed to be constant and equal to $C^{ext}_{Mg} \approx 0.35$. The penetration length, i.e. the distance from the boundary to the line where $C = \frac{C^{int}_{Mg} - C^{ext}_{Mg}}{2}$, is of the order of 30 µm

as the diffusing species, as (1) contrary to Fe and Mg, it is homogeneous in the reequilibrated grt II and (2) the compositional step between grt II and III is highest for Ca.

Considering Mg as the dependent component, Ca flux can be expressed as

$$J_{Ca} = -\left(D_{CaCa} + D_{CaFe}\frac{\partial C_{Fe}}{\partial C_{Ca}}\right)\frac{\partial C_{Ca}}{\partial x} = -D^{EB}_{Ca}\frac{\partial C_{Ca}}{\partial x}$$

where the effective binary diffusion coefficient is

$$D^{EB}_{Ca} = D_{CaCa} + D_{CaFe}\frac{\partial C_{Fe}}{\partial C_{Ca}}$$

Interdiffusion coefficients are related to self-diffusion coefficients by

$$D_{CaCa} = D^{*}_{Ca} - \frac{X_{Ca}D^{*}_{Ca}(D^{*}_{Ca} - D^{*}_{Mg})}{X_{Ca}D^{*}_{Ca} + X_{Fe}D^{*}_{Fe} + X_{Mg}D^{*}_{Mg}},$$

and

$$D_{CaFe} = -\frac{X_{Ca}D^{*}_{Ca}(D^{*}_{Fe} - D^{*}_{Mg})}{X_{Ca}D^{*}_{Ca} + X_{Fe}D^{*}_{Fe} + X_{Mg}D^{*}_{Mg}}$$

We used for this problem Ganguly et al.'s (1998) self-diffusion coefficients for Fe, Mg and Ca—they derived expressions for Fe and Mg and observed that $D^{*}_{Fe} \approx D^{*}_{Ca}$—yielding $D^{*}_{Fe} = D^{*}_{Ca} = 3.3 \times 10^{-24}$ m^2/s and $D^{*}_{Mg} = 5.3 \times 10^{-23}$ m^2/s. The values of D_{CaFe} are smaller by at least a factor of 2 than D_{CaCa}; furthermore, Fe-gradients are much smaller than Ca-gradients in the neighbourhood of grt II–III boundary. As a result, the terms $D_{CaFe}\frac{\partial C_{Fe}}{\partial C_{Ca}}$ can be neglected in the expression of D^{EB}_{Ca}, which therefore reduces to:

$$D^{EB}_{Ca} \simeq D_{CaCa}$$

The variations in D_{CaCa} within the composition range associated with the profiles are of the order of 30%, therefore modelling was carried out with an average value of $D^{EB}_{Ca} \simeq 5.3 \times 10^{-24}$ m^2/s.

The solution for the stair-like Ca profile is

$$X_{Ca}(x) = X^{eclo}_{Ca} + \frac{(X^{eclo}_{Ca} - X^{gran}_{Ca})}{2}\mathrm{erfc}\left(\frac{x}{2\sqrt{D^{EB}_{Ca}t}}\right)$$

where X^{eclo}_{Ca} and X^{gran}_{Ca} are respectively the Ca fraction of eclogite-facies garnet and inherited granulitic garnet

at $t = 0$ and $x = 0$ the grt II–III boundary. The fit between analysed Ca profiles and this simple solution is relatively good (Fig. 16); furthermore, the diffusion times computed from different profiles are well reproducible: for the three profiles, diffusion times range between 17 and 32 ky. The coefficients of Carlson (2006) are much more variable depending on garnet composition, from $D_{Ca}^{EB} \simeq D_{CaCa} = 2.5 \times 10^{-23}$ m^2/s for grt I to $D_{CaCa} = 2.38 \times 10^{-22}$ m^2/s in grt III. Although a proper modelling of diffusion profiles should incorporate variations of diffusion coefficients along a single profile, we can get rough estimates of the diffusion time by considering a constant coefficient equal to either one of these two values. As a result, the diffusion time is comprised in the range 140–2,900 years. These estimations evidence a very short time of residence at peak metamorphic conditions, preventing any effective grt II–III diffusion.

Tectonic interpretation of the two diffusion phases

The estimation of the duration of the two diffusion phases described above shows that while the diffusive reequilibration of inherited garnets lasted for several Ma, the main eclogite-facies crystallisation event was followed by a rapid exhumation, preventing large exchanges between granulitic garnets and eclogitic overgrowths. This chronology, as well as its good reproductibility between different samples, supports the idea that the main crystallisation event of eclogite-facies minerals was tectonically controlled and coincided with movement reversal, from burial to exhumation. We propose, therefore, that the onset of exhumation corresponds to some ''catastrophic'' event, associated to large deformation and fluid flow triggering rapid crystallisation of eclogite-facies minerals in the pervaded zone and followed by rapid exhumation.

Furthermore, the difference in diffusion extent between both phases implies that the unit reached slowly the *P–T* peak conditions during the end of its burial, before exhuming much faster. As no metamorphic phase has been recorded within the Holsnøy anorthosites up to peak eclogite-facies metamorphism, because of the anhydrous state of the granulite-facies protolith, the conditions of the Caledonian prograde path, in particular burial rates, are not known. Even the retrograde evolution is not well constrained, as there is still controversy over the age of both eclogite- and amphibolite-facies metamorphism (see Raimbourg et al. 2005a for a review). It must be noted that Perchuk (2002) has calculated very high exhumation rates for the same high-pressure unit, but on the basis of an assumption completely in disagreement with our study (grt II is considered as newly grown at eclogite-facies conditions). Exhumation rates calculated in terranes belonging to the nearby Western Gneiss region show really fast exhumation near HP or UHP metamorphism peak (8.1 mm/year in Moldefjord and 25 mm/year beneath Solund Basin, respectively recalculated from Terry et al. (2000) and Hacker et al. (2003) by Labrousse et al. (2004)). The very fast reverse movement in the first steps of exhumation is furthermore in agreement with results from mechanical modelling of subduction zones that we have carried out (Raimbourg et al. 2005b).

Conclusion

The petrographic study of garnet textures allows us to distinguish two separate phases within what was previously considered as a single event of eclogite-facies caledonian metamorphism. During the first phase, inherited granulitic garnets were fractured and reequilibrated, while during the second phase most eclogite-facies minerals, including garnet, were crystallised. Although *P–T* conditions can only be determined for the second phase (720°C and 20.5 kbars), the phase of garnet reequilibration is included in eclogite-facies metamorphism due to the systematic association between garnet fractures (with reequilibrated sides) and local eclogitisation extent.

Although equilibrium eclogite-facies garnets contain notably more Ca than inherited granulitic garnets, the observed reequilibration of the latter does not show any Ca input but only Fe^{2+}–Mg exchange. We discussed possible explanations for the lack in Ca reequilibration; the use of pseudosections led to discard thermodynamic reasons, variations in a_{H2O} or in reacting system. In agreement with compiled data from the literature, we propose that slow intra-garnet and intergranular transport properties of Ca compared to Fe/Mg prevented reequilibration in Ca.

Modelling of granulitic garnet diffusion profiles indicates that its reequilibration lasted for several My. On the contrary, profiles carried out across eclogite-facies and reequilibrated inherited garnets shows strong gradients, attesting to the small extent of diffusion and therefore the rapid exhumation that followed eclogite-facies minerals crystallisation. We propose the following scenario to account for these contrasted diffusion profiles: following the end of prograde motion, which was sufficiently slow to enable large garnet reequilibration, deformation and fluid flow associated with the geodynamical movement reversal

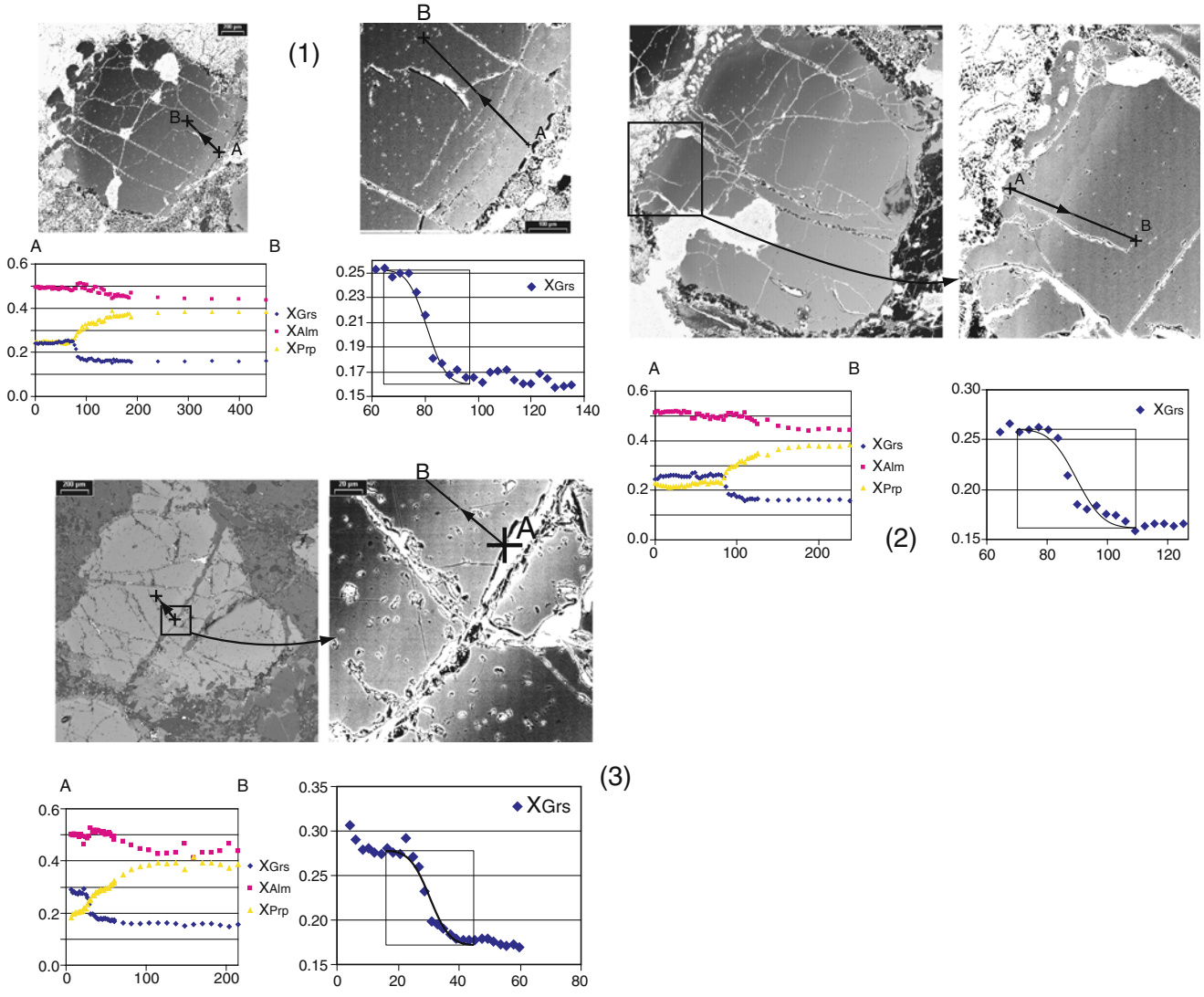

Fig. 16 Electron microprobe profiles across grt II–III boundary, where eclogite-facies garnet crystallised either as overgrowth on rims of granulitic garnets (1 and 2), or within fractures (3). Modelling of effective binary diffusion of Ca between adjacent grt II and III yielded diffusion times shorter than 100 ky

triggered eclogite-facies minerals crystallisation. The first steps of the subsequent exhumation were characterised by rapid uplift, preventing relaxation of garnet compositional heterogeneities.

Appendix: activity models

The following activity models were used to build the pseudosections:

White micas: Endmembers muscovite–paragonite–celadonite–ferroceladonite, non-ideal mixing with symmetric formalism interaction energies (Holland and Powell 1998).
Paragonite: Endmembers paragonite–margarite, mixing in the A site, no mixing in the tetrahedral site (Tinkham et al. 2001), from Thermocalc v2.7.
Amphibole: Endmembers tremolite–tschermakite–pargasite–ferroactinolite–glaucophane, non-ideal mixing with symmetric formalism interaction energies (adapted from Dale et al. 2000).
Clinopyroxene: P2/n omphacite is assumed, endmembers jadeite–diopside–hedenbergite–acmite, ideal mixing (Holland and Powell 1998).
Garnet: Endmembers grossular–almandin–pyrope–andradite, non-ideal mixing with symmetric formalism interaction energies (Holland and Powell 1998).
Orthopyroxene: Endmembers enstatite–ferrosilite–MgTschermak pyroxene (+ fictious ordered Fe–Mg pyroxene), non-ideal mixing with symmetric formalism interaction energies (Holland and Powell 1996a, b, 1998).

Epidotes: Endmembers clinozoisite–ferroepidote–epidote, non-ideal mixing with symmetric formalism interaction energies (Holland and Powell 1996a, b, 1998).

Analytical conditions and apparatus

Electronic microprobe: Two Cameca electron microprobes (CAMEBAX and SX50) available at Camparis (University Pierre et Marie Curie) using the wavelength dispersive technique with ZAF corrections. Operating conditions 15 kV and 10 nA.
BSE imaging: Annular Centaurus detector attached to a SEM Hitachi 2500 with a super Fevex-Sigma EDS system and a Quest Imaging software, available at Laboratoire de Geologie de l'Ecole Normale Supérieure de Paris. Operating conditions 20 kV and 0.5–5 nA.

References

Ai Y (1994) A revision of the garnet-clinopyroxene Fe2+-Mg exchange geothermometer. Contrib Mineral Petrol 115:467–473

Austrheim H (1987) Eclogitization of lower crustal granulites by fluid migration through shear zones. Earth Planet Sci Lett 81:221–232

Austrheim H (1990) The granulite-eclogite facies transition: A comparison of experimental work and a natural occurrence in the Bergen Arcs, western Norway. Lithos 25:163–169

Austrheim H (1998) Influence of fluid and deformation on metamorphism of the deep crust and consequences for the geodynamics of collision zones. In: Hacker BR, Liou JG (eds) When continents collide: geodynamics and geochemistry of ultrahigh-pressure rocks. Kluwer, The Netherlands, pp 297–323

Austrheim H, Griffin WL (1985) Shear deformation and eclogite formation within granulite-facies anorthosites of the Bergen Arcs, Western Norway. Chem Geol 50:267–281

Austrheim H, Mørk MBE (1988) The lower continental crust of the Caledonian mountain chain: evidence from former deep crustal sections in western Norway. Norges Geologiske Undersøkelse, Special publication 3:102–113

Austrheim H, Erambert M, Engvik AK (1997) Processing of crust in the root of the Caledonian continental collision zone: the role of eclogitization. Tectonophysics 273:129–153

Barrer RM, Bartholomew RF, Rees LVC (1963) Ion exchange in porous crystals. Part II. The relationship between self and exchange-diffusion coefficients. J Phys Chem Solids 24:309–317

Bejina F, Jaoul O, Liebermann (2003) Diffusion in minerals at high pressure: a review. Phys Earth Planet Int 139:3–20

Berman RG, Aranovich L, Pattison DR (1995) Reassessment of the garnet-clinopyroxene Fe-Mg exchange thermometer: II. Thermodynamic analysis. Contrib Mineral Petrol 119:30–42

Bingen B, Davis WJ, Austrheim H (2001) Zircon U-Pb geochronology in the Bergen arc eclogites and their Proterozoic protoliths, and implications for the pre-Scandian evolution of the Caledonides in western Norway. Geol Soc Am Bull 113(5):640–649

Bingen B, Austrheim H, Whitehouse MJ, Davis WJ (2004) Trace element signature and U-Pb geochronology of eclogite-facies zircon, Bergen Arcs, Caledonides of W Norway. Contrib Mineral Petrol 147:671–683

Boundy TM, Fountain DM, Austrheim H (1992) Structural development and petrofabrics of eclogite facies shear zones, Bergen Arcs, Western Norway: implications for deep crustal deformational processes. J Metamorph Geol 10:127–146

Boundy TM, Essene EJ, Hall CM, Austrheim H, Halliday AN (1996) Rapid exhumation of lower crust during continent-continent collision and late extension: Evidence from 40Ar/39Ar incremental heating of hornblendes and muscovites, Caledonian orogen, western Norway. Geol Soc Am Bull 108(9):1425–1437

Boundy TM, Hall CM, Li G, Essene EJ, Halliday AN (1997a) Fine-scale isotopic heterogeneities and fluids in the deep crust; a 40Ar/39Ar laser ablation and TEM study of muscovites from a granulite-eclogite transition zone. Earth Planet Sci Lett 148:223–242

Boundy TM, Mezger K, Essene EJ (1997b) Temporal and tectonic evolution of the granulite-eclogite association of the Bergen Arcs, western Norway. Lithos 39:159–178

Burton KW, O'Nions RK (1991) High-resolution garnet chronometry and the rates of metamorphic processes. Earth Planet Sci Lett 107:649–671

Carlson WD (1989) The significance of intergranular diffusion to the mechanisms and kinetics of porphyroblast crystallization. Contrib Mineral Petrol 103:1–24

Carlson WD (2002) Scales of disequilibrium and rates of equilibration during metamorphism. Am Mineral 87:185–204

Carlson WD (2006) Rates of Fe, Mg, Mn, and Ca diffusion in garnet. Am Mineral 91:1–11

Chakraborty S, Ganguly J (1990) Compositional zoning and cation diffusion in aluminosilicate garnets. In: Ganguly J (ed)) Diffusion, atomic ordering and mass transfer, vol 8. Advances in physical geochemistry. Springer, Berlin Heidelberg New York, pp 120–175

Chakraborty S, Ganguly J (1992) Cation diffusion in aluminosilicate garnets: experimental determination in spessartine-almandine diffusion couples, evaluation of effective binary diffusion coefficients, and applications. Contrib Mineral Petrol 111:74–86

Chakraborty S, Rubie DC (1996) Mg tracer diffusion in aluminosilicate garnets at 750–850°C, 1 atm. and 1300°C, 8.5 GPa. Contrib Mineral Petrol 122:406–414

Chernoff CB, Carlson WD (1997) Disequilibrium for Ca during growth of pelitic garnet. J Metamorph Geol 15:421–438

Chernoff CB, Carlson WD (1999) Trace element zoning as a record of chemical disequilibrium during garnet growth. Geology 27(6):555–558

Cohen AS, O'Nions RK, Siegenthaler R, Griffin WL (1988) Chronology of the pressure–temperature history recorded by a granulite terrain. Contrib Mineral Petrol 99:303–311

Crank J (1975) The mathematics of diffusion. Oxford University Press, Oxford, 414 pp

Cristensen JN, Rosenfeld J, DePaolo kDJ (1989) Rates of tectonometamorphic processes from rubidium and strontium isotopes in garnet. Science 244:1465–1469

Cygan RT, Lasaga AC (1985) Self-diffusion of magnesium in garnet at 750° to 950°C. Am J Sci 285:328–350

Dachs E, Proyer A (2002) Constraints on the duration of high-pressure metamorphism in the Tauern Window from diffusion modelling of discontinuous growth zones in eclogite garnet. J Metamorph Geol 20:769–780

Dale J, Holland TJB, Powell R (2000) Hornblende-garnet-plagioclase thermobarometry: a natural assemblage calibration of the thermodynamics of hornblende. Contrib Mineral Petrol 140:353–362

Dipple GM, Ferry JM (1992) Metasomatism and fluid flow in ductile fault zones. Contrib Mineral Petrol 112:149–164

Dodson M (1973) Closure temperature in cooling geochronological and petrological systems. Contrib Mineral Petrol 40:259–274

Dohmen R, Chakraborty S (2003) Mechanism and kinetics of element and isotopic exchange mediated by a fluid phase. Am Mineral 88:1251–1270

Droop GTR (1987) A general equation for estimating Fe3+ concentrations in ferromagnesian silicates and oxydes from microprobe analysis using stoechiometric criteria. Mineral Mag 51:431–435

Ellis DJ, Green DH (1979) An experimental study of the effect of Ca upon garnet-clinopyroxene Fe–Mg exchange equilibria. Contrib Mineral Petrol 71:13–22

Elphick SC, Ganguly J, Loomis TP (1985) Experimental determination of cation diffusivities in aluminosilicate garnets. Contrib Mineral Petrol 90:36–44

Elvevold S, Gilotti JA (2000) Pressure–temperature evolution of retrogressed kyanite eclogites, Weinschenk Island, North-East Greenland Caledonides. Lithos 53:127–147

Erambert M, Austrheim H (1993) The effect of fluid and deformation on zoning and inclusion patterns in poly-metamorphic garnets. Contrib Mineral Petrol 115:204–214

Florence FP, Spear FS (1995) Intergranular diffusion kinetics of Fe and Mg during retrograde metamorphism of a pelitic gneiss from the Adirondack Mountains. Earth Planet Sci Lett 134(3–4):329–340

Freer R, Edwards A (1999) An experimental study of Ca-(Fe,Mg) interdiffusion in silicate garnets. Contrib Mineral Petrol 134:370–379

Ganguly J, Tirone M (1999) Diffusion closure temperature and age of a mineral with arbitrary extent of diffusion: theoretical formulation and applications. Earth Planet Sci Lett 170:131–140

Ganguly J, Chakraborty S, Sharp TG, Rumble III D (1996) Constraint on the time scale of biotite-grade metamorphism during Acadian orogeny from a natural garnet–garnet diffusion couple. Am Mineral 81:1208–1216

Ganguly J, Cheng W, Chakraborty S (1998) Cation diffusion in aluminosilicate garnets: experimental determination in pyrope–almandine diffusion couples. Contrib Mineral Petrol 131:171–180

Getty S, Selverstone J, Wernicke BP, Jacobsen SB, Aliberti E, Lux DR (1993) Sm-dating of multiple garnet growth events in an arc-continent collision zone, northwestern US Cordillera. Contrib Mineral Petrol 115:45–57

Glodny J, Kühn A, Austrheim H (2002) Rb/Sr record of fluid-rock interaction in eclogites, Bergen Arcs, Norway. Geochim Cosmochim Acta 66(15A):A280

Hacker BR, Andersen TB, Root DB, Mehl L, Mattinson JM, Wooden JL (2003) Exhumation of high-pressure rocks beneath the Solund Basin, Western Gneiss Region of Norway. J Metamorph Geol 21:613–629

Hauzenberger CA (2005) Garnet zoning in high pressure granulite-facies metapelites, Mozambique belt, SE-Kenya: constraints on the cooling history. Eur J Mineral 17(1):43–55

Holland TJB, Powell R (1990) An enlarged and updated internal consistent dataset with incertainties and correlations: the system K_2O – Na_2O – CaO – MgO – MnO – FeO – Fe_2O_3 – Al_2O_3 – TiO_2 – C – H_2O – O_2. J Metamorph Geol 8:89–124

Holland TJB, Powell R (1996a) Thermodynamics of order–disorder in minerals 1: symmetric formalism applied to minerals of fixed composition. Am Mineral 81:1413–1424

Holland TJB, Powell R (1996b) Thermodynamics of order–disorder in minerals 2: symmetric formalism applied to solid solutions. Am Mineral 81:1425–1437

Holland TJB, Powell R (1998) An internally-consistent thermodynamic data set for phases of petrological interest. J Metamorph Geol 16:309–343

Hollister LS (1966) Garnet zoning—an interpretation based on Rayleigh fractionation model. Science 154:1647–1651

Indares A (1995) Metamorphic interpretation of high pressure-temperature metapelites with preserved growth zoning in garnet, eastern Grenville Province, Canadian Shield. J Metamorph Geol 13:475–486

Jamieson RA, O'Beirne-Ryan AM (1991) Decompression-induced growth of albite porphyroblasts, Fleur de Lys Supergroup, western Newfoundland. J Metamorph Geol 9:433–439

Jamtveit B, Bucher-Nurminen K, Austrheim H (1990) Fluid controlled eclogitization of granulites in deep crustal shear zones, Bergen arcs, Western Norway. Contrib Mineral Petrol 104:184–193

Johnson JW, Oelkers EH, Helgeson HC (1992) SUPCRT92—a software package for calculating the standard molal thermodynamic properties of minerals, gases, aqueous species, and reactions from 1-bar to 5000-bar and 0°C to 1000°C. Comput Geosci 18(7):899–947

Kolderup CF, Kolderup NH (1940) Geology of the Bergen Arc System vol 20, vol 20. Bergens Museum Skrifter, 137 pp

Konrad-Schmolke M, Handy MR, Babist J, O'Brien PJ (2005) Thermodynamic modelling of diffusion-controlled granet growth. Contrib Mineral Petrol 149(2):181–195

Krogh Ravna EJ (2000a) Distribution of Fe2+ and Mg between coexisting garnet and hornblende in synthetic and natural systems: an empirical calibration of the garnet-hornblende Fe–Mg geothermometer. Lithos 53(3–4):265–277

Krogh Ravna EJ (2000b) The garnet-clinopyroxene Fe2+-Mg geothermometer: an updated calibration. J Metamorph Geol 18:211–219

Kühn A (2002) The influence of fluid on the granulite to eclogite and amphibolite facies transition: a study in the anorthositic rocks from the Lindås Nappe, Bergen Arcs, West Norway. Unpublished Ph.D. thesis, University of Oslo, 330 pp

Labrousse L, Jolivet L, Andersen TB, Agard P, Maluski H, Schärer U (2004) Pressure–temperature–time-deformation history of the exhumation of ultra-high-pressure rocks in the Western Gneiss Region, Norway. GSA Spec Pap 380:155–183

Lang HM, Gilotti JA (2001) Plagioclase replacement textures in partially eclogitised gabbros from the Sanddal mafic-ultramafic complex, Greenland Caledonides. J Metamorph Geol 19:497–517

Lasaga AC (1979) Multicomponent exchange and diffusion in silicates. Geochim Cosmochim Acta 43:455–469

Lasaga AC (1983) Geospeedometry: an extension of geothermometry. Kinetics and equilibrium in mineral reactions. Adv Phys Geochem 3:81–114

Loomis TP (1982) Numerical simulation of the disequilibrium growth of garnet in chlorite-bearing aluminous pelitic rocks. Can Mineral 20:411–423

Loomis TP, Ganguly J, Elphick SC (1985) Experimental determination of cation diffusivities in aluminosilicate garnets. Contrib Mineral Petrol 90:45–51

Marmo BA, Clarke GL, Powell R (2002) Fractionation of bulk rock composition due to porphyroblast growth: effects on eclogite facies mineral equilibria, Pam Peninsula, New Caledonia. J Metamorph Geol 20:151–165

Mattey D, Jackson DH, Harris BW, Kelly S (1994) Isotopic constraints on fluid infiltration from an eclogite facies shear zone, Holsnøy, Norway. J Metamorph Geol 12:311–325

Mezger K, Hanson GN, Bohlen SR (1989) U–Pb systematics of garnet: dating the growth of garnet in the Late Archean Pikwitonei granulite domain at Cauchon and Natawahunan, Manitoba, Canada. Contrib Mineral Petrol 101:136–148

O'Brien PJ (1997) Garnet zoning and reaction textures in overprinted eclogites, Bohemian Massif, European Variscides: a record of their thermal history during exhumation. Lithos 41:119–133

O'Brien PJ (1999) Asymmetric profiles in garnet from HP-HT granulite and implications for volume and grain-boundary diffusion. Mineral Mag 63(2):227–238

O'Brien PJ, Vrana S (1995) Eclogites with a short-lived granulite facies overprint in the Moldanubian Zone, Czech Republic: petrology, geochemistry and diffusion modelling of garnet zoning. Geol Rundsch 84:473–488

Perchuk AL (2002) Eclogites of the Bergen Arcs complex, Norway: petrology and mineral chronometry. Petrologiya 10(2):115–137

Perchuk A, Philippot P, Erdmer P, Fialin M (1999) Rates of thermal equilibration at the onset of subduction deduced from diffusion modeling of eclogitic garnets, Yukon-Tanana terrane, Canada. Geology 27(6):531–534

Powell R (1985) Regression diagnostics and robust regression in geothermometer/geobarometer calibration: the garnet–clinopyroxene geothermometer revisited. J Metamorph Geol 3:327–342

Powell R, Holland TJB (1988) An internally consistent dataset with uncertainties and correlations: 3. Applications to geobarometry, worked examples and a computer program. J Metamorph Geol 6:173–204

Ragnhildsveit J, Helliksen D (1997) Geologisk kart over Norge, begrunnskart Bergen, 1:250000. In: Norges Geologiske Undersøkelse

Raimbourg H (2005) Mécanismes d'éclogitization et conséquences pour l'exhumation des roches métamorphiques de haute pression. Unpublished Ph.D. thesis, University Pierre et Marie Curie, 407 pp

Raimbourg H, Jolivet L, Labrousse L, Leroy YM, Avigad D (2005a) Kinematics of syneclogite deformation in the Bergen Arcs, Norway: implications for exhumation mechanisms. In: Gapais D, Brun JP, Cobbold PR (eds) Deformation Mechanisms, Rheology and Tectonics: from Minerals to the Lithosphere, vol 243. Geological Society, London, Special Publications, pp 175–192

Raimbourg H, Jolivet L, Leroy Y, Labrousse L (2005b) Consequences of progressive eclogitization on crustal exhumation, a mechanical study. Geophys J Int (in press)

Roberts D, Gee DG (1985) An introduction to the structure of the Scandinavian Caledonides. In: Gee DG, Sturt BA (eds) The Caledonide Orogen: Scandinavia and related areas, vol 1. Wiley, Chichester, pp 55–68

Schmid R, Altenberger U, Oberhansli R (1998) Polyphase tectonometamorphic evolution of the northwestern Lindås Nappe on Holsnøy, Bergen Arcs, Caledonides, S-W Norway. Zbl Geol Paläont Teil I 1–2:1–18

Schwandt CS, Cygan RT, Westrich HR (1995) Mg self-diffusion in pyrope garnet. Am Mineral 80:483–490

Schwandt CS, Cygan RT, Westrich HR (1996) Ca self-diffusion in grossular garnet. Am Mineral 81:448–451

Spear FS, Daniel CG (2001) Diffusion control of garnet growth, Harpswell Neck, Maine, USA. J Metamorph Geol 19:179–195

Stüwe K (1997) Effective bulk composition changes due to cooling: a model predicting complexities in retrograde reaction textures. Contrib Mineral Petrol 129:43–52

Svensen H, Jamtveit B, Yardley B, Engvik AK, Austrheim H, Broman C (1999) Lead and bromine enrichment in eclogite-facies fluids: extreme fractionation during lower-crustal hydration. Geology 27(5):467–470

Svensen H, Jamtveit B, Banks DA, Austrheim H (2001) Halogen contents of eclogite facies fluid inclusions and minerals: Caledonides, western Norway. J Metamorph Geol 19:165–178

Terry MP, Robinson P, Hamilton M, Jercinovic MJ (2000) Monazite geochronology of UHP and HP metamorphism, deformation, and exhumation, Nordøyane; Western Gneiss Region, Norway. Am Mineral 85:1651–1664

Tinkham DK, Zuluaga CA, Stowell HH (2001) Metapelite phase equilibria modeling in MnNCKFMASH: the effect of variable $_2O_3$ and MgO/(MgO+FeO) on mineral stability. Geol Mater Res 3(1):1–42

Vance D, O'Nions RK (1990) Isotopic chronometry of zoned garnets: growth kinetics and metamorphic histories. Earth Planet Sci Lett 97:227–240

Vance D, Strachan RA, Jones KA (1998) Extensional versus compressional settings for metamorphism: garnet chronometry and pressure–temperature–time histories in the Moine Supergroup, northwest Scotland. Geology 26(10):927–930

Waters DJ, Martin HN (1993) Geobarometry in phengite-bearing eclogites. Terra Abstr 5:410–411